

High-resolution distributions of $\Delta(\text{O}_2/\text{Ar})$ on the northern slope of the South China Sea and estimates of net community production

Chuan Qin^{1,2}, Guiling Zhang^{1,2,*}, Wenjing Zheng¹, Yu Han^{1,3}, Sumei Liu^{1,2}

1. Key Laboratory of Marine Chemistry Theory and Technology, Ministry of Education/Institute for Advanced Ocean Study, Ocean University of China, 238 Songling Road, 266100 Qingdao, P. R. China

2. Laboratory for Marine Ecology and Environmental Science, Qingdao National Laboratory for Marine Science and Technology, Qingdao 266237, P. R. China

3. Hainan Tropical Ocean University, Sanya 572022, P. R. China

* Correspondence to: Guiling Zhang (guilingzhang@ouc.edu.cn)

Abstract

Dissolved oxygen-to-argon ratios (O_2/Ar) in the oceanic mixed layer has been widely used to estimate net community production (NCP), which is the difference between gross primary production and community respiration and is a proxy of carbon export from the surface ocean. In order to obtain the high-resolution distribution of NCP and improve our understanding of its regulating factors in the slope region of the Northern South China Sea (SCS), we conducted continuous measurements of dissolved O_2 , Ar, and CO_2 by membrane inlet mass spectrometry during two cruises in October 2014 and June 2015. An overall autotrophic condition was observed in the study region in both cruises with an average $\Delta(\text{O}_2/\text{Ar})$ of 1.1 % \pm 0.9 % in October 2014 and 2.7 % \pm 2.8 % in June 2015. NCP was on average 11.5 ± 8.7 mmol C m^{-2} d^{-1} in October 2014 and 11.6 ± 12.7 mmol C m^{-2} d^{-1} in June 2015. Correlations between dissolved inorganic nitrogen (DIN), $\Delta(\text{O}_2/\text{Ar})$, and NCP were observed in both cruises, indicating that NCP is subject to the nitrogen limitation in the study region. In June 2015, we observed a rapid response of the ecosystem to the episodic nutrient supply induced by eddies. Eddy-entrained shelf water intrusion, which supplied large amounts of terrigenous nitrogen to the study region, promoted NCP in the study region by 376 %. In addition, upwelling brought large uncertainties to the estimation of NCP at the core region of the cold eddy (cyclone) in June 2015. The deep euphotic depth in the SCS and the absence of correlation between NCP and the average photosynthetically available radiation (PAR) in the mixed layer in the autumn indicate that light availability may not be a significant limitation on

NCP in the SCS. This study helps to understand the carbon cycling in the highly dynamic shelf system.

Keywords: O₂/Ar; Net community production; Nutrients; Eddy; Northern slope of South China Sea

1. Introduction

The oceanic carbon sequestration is partially regulated by the production and export process of biological organic carbon in the surface ocean. Net community production (NCP) corresponds to gross primary production (GPP) minus community respiration (CR) in the water (Lockwood et al., 2012) and is an important indicator of carbon export. At steady state, NCP is equivalent to the rate of organic carbon export and transfer up the food web, which can quantify the strength of biological pump (Lockwood et al., 2012). Dissolved oxygen-to-argon ratio (O₂/Ar) has been developed as a proxy for NCP in a water mass based on the similar physical properties of O₂ and Ar (Craig and Hayward, 1987; Kaiser et al., 2005). The biological production in the open oceans (i.e., Southern Ocean, Pacific, Arctic Ocean) has been inferred using the O₂/Ar ratio to estimate NCP in numerous researches (e.g., Hamme et al., 2012; Lockwood et al., 2012; Ulfsbo et al., 2014; Shadwick et al., 2015; Stanley et al., 2010). During recent years, several high-resolution measurements of O₂/Ar and NCP in coastal waters have been reported (Tortell et al., 2012; Tortell et al., 2014; Eveleth et al., 2017; Izett et al., 2018). Despite the coastal waters such as shelves and estuaries only account for 7 % of the global ocean surface area, they are known to contribute to 15–30 % of the total oceanic primary production (Bi et al., 2013; Cai et al., 2011) and play an important role in marine carbon cycle and production. However, these regions still suffer from low resolution measurements and are poorly represented in global NCP data sets.

The South China Sea (SCS) is one of the largest marginal seas in the world with extremely complex ecological characteristics. River runoff from the Pearl and Mekong Rivers introduces large amounts of dissolved nutrients into the SCS (Ning et

al., 2004). Due to the influence of seasonal monsoons, the surface circulation in the SCS changes from a basin-scale cyclonic gyre in winter to an anticyclonic gyre in summer (Hu et al., 2000). The surface water masses on the northern slope of SCS can be categorized into three regimes: shelf water, offshore water (e.g., the intruded Kuroshio water), and the SCS water (Feng, 1999; Li et al., 2018). The shelf water is mixed with fresh water from rivers or coastal currents and thus usually has low salinity ($S < 33$) and low density (Uu and Brankart, 1997; Su and Yuan, 2005; Cheng et al., 2014). Both offshore water and SCS water originate from the Northern Pacific. Thus offshore water has similar hydrographic characteristics of high temperature and high salinity as the Northern Pacific water. But the SCS water has changed a lot in its hydrographic property because of the mixing processes, heat exchange and precipitation during its long residence time in the SCS (Feng et al., 1999; Li et al., 2018). The distributions of phytoplankton and primary productivity of the SCS show great temporal and spatial variation (Ning et al., 2004). Low chlorophyll a (Chl a) and primary production are the significant characteristics of the SCS basin which is considered an oligotrophic region, and macronutrients (i.e. nitrogen) are the main limitations of phytoplankton growth and productivity (Ning et al., 2004; Lee Chen, 2005; Han et al., 2013). The excessive runoff from Pearl River can result in high N/P (nitrogen/phosphorus) ratio of > 100 , shifting the nutritive state from nitrogen deficiency to phosphorus deficiency in the coastal region of SCS (Lee Chen and Chen, 2006). Dissolved iron is also a potential limitation on primary production, especially in the high nutrient low chlorophyll (HNLC) regions (Cassar et al., 2011). But on the northern slope of SCS, the concentration of dissolved iron is high enough to support the growth of phytoplankton in the surface water (Zhang et al., 2019). The northern slope of SCS is an important transition region between coastal area and SCS basin. In the summer, the shelf water intrusion is an important process changing the nutritive state in the northern slope region of SCS (He et al., 2016; Lee Chen and Chen, 2006). But so far, the NCP enhancement caused by this process is still unknown.

Previous studies about the organic carbon export in the SCS were mostly conducted on particulate organic carbon (POC) flux (e.g., Bi et al., 2013; Cai et al., 2015; Chen

et al., 1998; Chen et al., 2008; Ma et al., 2008; Ma et al., 2011). Little research has been conducted on NCP in the SCS to date. Chou et al. (2006) estimated NCP in the northern SCS during the summertime to be $4.47 \text{ mmol C m}^{-2} \text{ d}^{-1}$ based on the time change rate of dissolved inorganic carbon (DIC) in the mixed layer at the South East Asia Time-Series Station (SEATS) from 2002 to 2004. Wang et al. (2014) used GPP and community respiration data from a light/dark bottle incubation experiment to calculate NCP in the northern SCS and obtained a range from -179.0 to $377.6 \text{ mmol O}_2 \text{ m}^{-2} \text{ d}^{-1}$ (-129.7 to $273.6 \text{ mmol C m}^{-2} \text{ d}^{-1}$). Huang et al. (2018) estimated monthly NCP from July 2014 to July 2015 based on in situ O_2 measurements on an Argo profiling float and reported the cumulative NCP to be $0.29 \text{ mol C m}^{-2} \text{ month}^{-1}$ ($9.67 \text{ mmol C m}^{-2} \text{ d}^{-1}$) during the northeast monsoon period and $0.17 \text{ mol C m}^{-2} \text{ month}^{-1}$ ($5.67 \text{ mmol C m}^{-2} \text{ d}^{-1}$) during the southwest monsoon period in the SCS basin. However, most of these studies in the SCS were constrained by methodological factors attributed to discrete sampling and cannot reveal the rapid productivity response to highly dynamic environmental fluctuations of coastal systems. Discrete sampling suffers from low spatial resolution, and cannot adequately resolve variabilities caused by small-scale physical or biological processes in dynamic marine systems. In addition, each of the three methods for NCP estimate mentioned above has its limitation. DIC-based NCP estimate is not suitable for the coastal region, because instead of biological metabolism, the terrestrial runoff can be the strongest factor influencing the DIC in the coastal system (Mathis et al., 2011). The unavoidable difference between in situ circumstance and on deck incubation condition can introduce uncertainties to the NCP derived from light/dark bottle incubation (Grande et al., 1989). Though Argo profiling float partly gets rid of the limitation of discrete sampling, it's hard to control its movement in the study region. However, no high-resolution measurement of NCP has been reported for the SCS so far.

In this paper, we present high-resolution NCP estimates in the northern slope region of the South China Sea based on continuous shipboard dissolved O_2/Ar measurements. We discuss the regulating factors of NCP based on ancillary measurements of other hydrographic parameters. Our high-resolution measurements caught the rapid

response of the ecosystem to the episodic nutrient supply induced by eddies and help us to quantify the contribution of eddy-entrained shelf water intrusion to NCP in the summer cruise.

2. Methods

2.1 Continuous underway sampling and measurement

Continuous measurements of dissolved O₂, Ar, and CO₂ were obtained using membrane inlet mass spectrometry (MIMS, HPR 40, Hiden Analytical, UK) (Tortell, 2005) onboard the *RV 'Nanfeng'* during two cruises in the northern slope region of the South China Sea (Figures 1a, 1b) from 13 to 23 October 2014 and from 13 to 29 June 2015. In addition, a cyclonic-anticyclonic eddy pair was observed in June 2015 (Figure 1c) and resulted in dramatic influences on the study region.

We developed a continuous shipboard measurement system of dissolved gases following the method described by Guéguen and Tortell (2008). Surface seawater was collected continuously using the ship's underway intake system (~5 m depth) and was divided into different lines for various underway scientific measurements. Seawater from the first line passed through a chamber at a flowrate of 2–3 L min⁻¹ to remove macroscopic bubbles and to avoid pressure bursts. A flow of ~220 mL min⁻¹ was continuously pumped from the chamber using a Masterflex Peristaltic Pump equipped with L/S® multichannel cartridge pump heads (Cole Parmer). In order to minimize the O₂/Ar fluctuations due to temperature effects and water vapor pressure variations, the water samples flowed through a stainless steel coil (~6 m) with 0.6 mm wall thickness immersed in a water bath (Shanghai Bilon Instrument Co. Ltd, China) to achieve a constant temperature (~2 °C below the sea surface temperature), which avoided temperature-induced supersaturation and subsequent bubble formation. Then the water samples were introduced into a cuvette with a silicone membrane mounted on the inside. The analyte gases were monitored by a Faraday cup detector in the vacuum chamber after diffusion through the silicone membrane, and the signal intensities at the relevant mass to charge (m/z) ratios (32, 40 and 44 for O₂, Ar and

CO₂, respectively) were recorded by MASsoft. Based on the continuous measurement of 50 L air-equilibrated seawater, the long-term signal stability (measured as the coefficient of variation) over 12 h was 1.57 %, 3.75 % and 2.21 % for O₂, Ar and CO₂, respectively. Seawater from the second line passed through a flow chamber, where an RBR Maestro (RBR, Canada) was installed to continuously record temperature, salinity, dissolved oxygen (DO), and Chl a. We didn't obtain continuous DO data in October 2014 because the DO sensor of RBR broke down during this cruise. A third line was used to drain the excess seawater. Underway pipelines were flushed with freshwater or bleach every day, to avoid possible in-lines biofouling. The data from the underway transects were exported to spreadsheets and compiled into 5 min averages, and the comparisons of the gas data with other hydrographic variables were based on the UTC time recorded for each measurement.

The O₂/Ar ratio measurements were calibrated with air-equilibrated seawater samples at about 6–8 h intervals to monitor instrument drift and calculate $\Delta(\text{O}_2/\text{Ar})$. These air-equilibrated seawater samples were prefiltered (0.22 μm) and bubbled with ambient air for at least 24 h to reach equilibrium at sea surface temperature (Guéguen and Tortell, 2008). For calibration, 800 mL of air-equilibrated seawater sample was transferred into glass bottles and immediately drawn into the cuvette, where the first 200 mL of the sample was used to flush the cuvette and pipelines. After 3 min recirculation of the sample, the average signal intensity was obtained to calculate O₂/Ar. During the course of measurements, flow rate and the temperature of water bath were both kept the same as the underway measurements. The precision of MIMS-measured O₂/Ar was 0.22 %, based on analyses of 20 duplicate samples in the laboratory test, which is comparable to previous studies and sufficient to detect biologically driven gas fluctuations in seawater (Tortell, 2005).

The instrumental CO₂ ion current was calibrated at about 12–24 h intervals using equilibrated seawater standards as per Guéguen and Tortell (2008) during the survey in June 2015. Prefiltered seawater (0.22 μm) was gently bubbled with dry CO₂ standards (200, 400, and 800 ppm, provided by the Chinese National Institute of Metrology) at in situ temperature. After 2 days of equilibrium, these standards were

analyzed by MIMS following the same procedure for measuring air-equilibrated seawater samples to obtain a calibration curve between CO₂ signal intensity and mole fraction. The reproducibility of these measurements was better than 5 % within 15 days. Then we used the empirical equations reported by Takahashi et al. (2009) to convert the CO₂ mole fraction derived from the calibration curve to the in situ partial pressure of CO₂ ($p\text{CO}_2$).

Chlorophyll-a (Chl a) data from the RBR sensor were linear calibrated against extracted Chl a measurements of discrete seawater samples taken from the same seawater outlet as for MIMS measurements. Samples were filtered through polycarbonate filters (0.22 μm). The filter membranes were then packed with pre-sterilized aluminum foil and stored in a freezer ($-20\text{ }^\circ\text{C}$) until extraction by acetone and analysis using a fluorimetric method (F-4500, HITACHI, Japan) described by Parsons (1984). The mean residual of this calibration was $0.00 \pm 0.07\text{ }\mu\text{g L}^{-1}$.

2.2 Estimation of NCP based on O₂/Ar measurements

NCP in the mixed layer was estimated by the O₂/Ar mass balance from continuous measurements. Due to similar physical properties of O₂ and Ar, $\Delta(\text{O}_2/\text{Ar})$ is used as a proxy of the biological O₂ supersaturation and is defined as (Craig and Hayward, 1987):

$$\Delta(\text{O}_2 / \text{Ar}) = \frac{([\text{O}_2]/[\text{Ar}])}{([\text{O}_2]/[\text{Ar}])_{\text{eq}}} - 1$$

where $[\text{O}_2]/[\text{Ar}]$ is the measured dissolved O₂/Ar ratio of the mixed layer and $([\text{O}_2]/[\text{Ar}])_{\text{eq}}$ is the measured dissolved O₂/Ar ratio of the air-equilibrated seawater samples. $\Delta(\text{O}_2/\text{Ar})$ is the percent deviation of the measured O₂/Ar ratio from the equilibrium. Assuming a steady state and negligible physical supply, NCP is the air-sea biological O₂ flux and can be estimated as (Reuer et al., 2007):

$$\text{NCP} (\text{mmol C m}^{-2} \text{ d}^{-1}) \approx k_{\text{O}_2} \cdot [\text{O}_2]_{\text{sat}} \cdot \Delta(\text{O}_2 / \text{Ar}) \cdot r_{\text{C:O}_2} \cdot \rho$$

where k_{O_2} is the weighted gas transfer velocity of O₂ (m d^{-1}); $[\text{O}_2]_{\text{sat}}$ denotes the saturation concentration of dissolved O₂ ($\mu\text{mol kg}^{-1}$) in the mixed layer, which is

calculated based on temperature and salinity (Weiss, 1970); $r_{C:O_2}$ is the photosynthetic quotient of C and O₂ and was reported as 1:1.38 in the SCS (Jiang et al., 2011); ρ is seawater density in units of kg m⁻³ (Millero and Poisson, 1981). We estimated k_{O_2} using the European Centre for Medium-Range Weather Forecasts (ECWMF) wind-speed reanalysis data product with a 0.25° × 0.25° grid (<https://www.ecmwf.int>), the parameterization by Wanninkhof (1992), and the gas exchange weighting algorithm by Teeter et al. (2018). Teeter et al., (2018) pointed out that modern O₂/Ar method does not strongly rely on the steady state assumption. When this assumption is violated, our estimate does not represent the actual daily NCP but rather an estimate of NCP weighted over the residence time of O₂ in the mixed layer and along the path of the water parcel during that period. Thus the residence time of O₂ in the mixed layer is an important implication of the weighted timescale of NCP before the measurement of O₂/Ar. The residence time of O₂ (τ , d) in the mixed layer is estimated as the ratio of mixed layer depth (MLD, m) to gas transfer velocity of O₂ (k_{O_2} , m d⁻¹) (Jonsson et al., 2013).

2.3 Ancillary measurements and calculations

Surface water samples for the nutrient analysis were collected from Niskin bottles mounted on the CTD, where the samples were filtered through acid-cleaned acetate cellulose filters (pore size: 0.4 μ m). The filtrates were poisoned by HgCl₂ and stored in the dark at 4 °C. In the laboratory, the nutrients were determined photometrically by an auto-analyzer (QuAatro, SEAL Analytical, Germany) with a precision better than 3 %. The MLDs were defined by the $\Delta\sigma_t = 0.125$ kg m⁻³ criterion (Monterey and Levitus, 1997). The subsurface chlorophyll maximum layer (SCML) was observed using the fluorescence sensor mounted on the CTD, and it usually occurs at the bottom of euphotic layer (Hanson et al., 2007; Liao et al., 2018; Teira et al., 2005). Because no PAR (Photosynthetically Available Radiation) data were obtained in two cruises, we decided to regard the depth of SCML as the euphotic depth (Z_{eu}). The MLDs and the SCML were calculated at the stations where the vertical CTD casts were made. The MLDs for underway data between CTD stations was calculated using

linear interpolation based on the distance between the underway points and nearest CTD stations. We matched the underway data to each CTD location using a combination of latitude/longitude threshold (latitude/longitude of CTD station $\pm 0.05^\circ$) and time threshold (end/start of stationary time ± 1 h), then took the averages of these underway data for further analysis with discrete nutrient concentrations.

The daily satellite chlorophyll data were obtained from the Copernicus website (<https://resources.marine.copernicus.eu>). The product we used was provided by ACRI-ST company (Sophia Antipolis, France), with a space-time interpolation (the “Cloud Free”). Daily and 8-day PAR data collected by MODIS-Aqua sensor were obtained from NASA’s ocean color website (<https://oceancolor.gsfc.nasa.gov/l3>). The spatial resolution of both satellite products is 4 km, and we match the satellite PAR with CTD station by choosing the closet PAR data point to the CTD location. A light attenuation coefficient (K_d , m^{-1}) was used to estimate the average PAR in the mixed layer (Kirk 1994; Jerlov 1976):

$$K_d = \frac{4.605}{Z_{eu}}$$

3. Results and Discussion

3.1 Distributions of hydrographic parameters and gases

The distributions of temperature, salinity, Chl a, and $\Delta(O_2/Ar)$ during the autumn cruise (October 2014) are shown in Figure 2. Sea surface temperature (SST) ranged from 26.96 °C to 28.53 °C with an average of 27.82 ± 0.33 °C. Sea surface salinity (SSS) ranged from 33.28 to 34.11 with the low values occurring in the southeast of the region. Chl a concentration ranged from 0.01 to 0.71 $\mu g L^{-1}$ and was in an average of 0.18 ± 0.13 $\mu g L^{-1}$, which was comparable to the 11-year mean value (~ 0.2 $mg m^{-3}$) in the same region in October reported by Liu et al. (2014). $\Delta(O_2/Ar)$ values were in the range of -2.9 – 4.9 % (avg. 1.1 % ± 0.9 %) and most areas were slightly oversaturated (Figure 2d). In addition, please note that all averages we have published in this paper are reported in the format of *mean \pm standard deviation*.

In June 2015, SST ranged from 29.28 °C to 32.24 °C and was in an average of 30.88

± 0.59 °C (Figure 3a). SSS ranged from 30.81 to 34.16. Transect 3 was significantly characterized by low salinity (Figure 3b). He et al (2016) reported that this phenomenon was influenced by the eddy-entrained Pearl River plume (shelf water) injected into the SCS. Chl *a* varied in a range of 0.09–0.58 $\mu\text{g L}^{-1}$ in the study region. Under the influence of this plume water, Chl *a* values higher than 0.30 $\mu\text{g L}^{-1}$ were observed along Transect 3 (Figure 3c). In contrast, Chl *a* was in the range of 0.09–0.18 $\mu\text{g L}^{-1}$ along Transect 1 and 2. It was obvious that DO was much higher in the east side than the west side in the study region (Figure 3d). $\Delta(\text{O}_2/\text{Ar})$ ranged from –3.9–13.6 %. Most of the $\Delta(\text{O}_2/\text{Ar})$ values were positive in the study region (avg. 2.7 % ± 2.8 %), whereas the negative values were concentrated along Transect 4 (Figure 3f). $\Delta(\text{O}_2/\text{Ar})$ along Transect 3 was in an average of 7.2 % ± 2.6 %, significantly higher than that of other transects (Figure 3f). $p\text{CO}_2$ exhibited a high degree of spatial and temporal variability and the high values mostly occurred on the west side of the study region (Figure 3e). Resulting from the considerable low $p\text{CO}_2$ in Transect 3, the average $p\text{CO}_2$ (323 ± 93 μatm) in the study region was lower than those reported previously, i.e., 350–370 μatm by Zhai et al (2009) and 340–350 μatm by Rehder and Sues (2001). Due to the influence of the plume water, the average $p\text{CO}_2$ in Transect 3 was 222 ± 33 μatm , with a range of 144–321 μatm . In the summer, shelf water mixed with Pearl River plume is the most important factor influencing $p\text{CO}_2$ in the coastal and shelf region of northern SCS, which can result in the $p\text{CO}_2$ values as low as 150 μatm (Li et al., 2020). Here we apply an average atmospheric $p\text{CO}_2$ of 382 μatm that observed in July 2015 in the northern SCS (Li et al., 2020) to calculate the $p\text{CO}_2$ difference ($\Delta p\text{CO}_2$) between the surface water and the atmosphere. $\Delta p\text{CO}_2$ ranged from –238 to –61 μatm along Transect 3, indicative of a strong CO_2 sink.

3.2 Mixed layer depth, euphotic depth and residence time of O_2 in the mixed layer

The mixed layer depth (MLD), euphotic depth (Z_{eu}) and residence time of O_2 (τ) in the mixed layer at CTD stations of two cruises are shown in Table 1 and 2 respectively. In autumn 2014, MLD ranged from 27 to 81 m, with an average of $55 \pm$

15 m (Table 1). The average Z_{eu} was 74 ± 12 m, approximately 20 m deeper than MLD (Table 1). The residence time of O_2 in the mixed layer ranged from 3 to 13 d (Table 1), comparable to a reasonable range of 1–2 weeks reported by previous studies (Izett et al., 2018; Manning et al., 2017). The average residence time of O_2 was 9 ± 3 d, indicating that our estimate generally quantified NCP over 9 days prior to the underway observation of O_2/Ar in the mixed layer during this cruise.

The average MLD in June 2015 was just 18 ± 6 m, shallower than that of October 2014 (Table 2). Significant shallow MLD occurred at two stations (J-10, J-11) located in Transect 3 (Table 2, Figure S1f). The low-salinity shelf water intrusion is the main cause of this shallow MLD of 8 m. The average Z_{eu} was 58 ± 18 m, approximately 40 m deeper than the MLD (Table 2). The residence time of O_2 in the mixed layer ranged from 2 to 12 d (Table 2), indicating a fast gas exchange in some stations. In addition, we also observed relatively obvious subsurface O_2 maxima in Transect 1 and 2 in summer 2015. But this phenomenon didn't exist in autumn 2014.

In both cruises, the Z_{eu} was observed obviously deeper than MLD. This result partly suggests that light availability may not be a limitation of NCP in the northern slope of SCS. Especially in the summer, Z_{eu} extended to 2–7 times of MLD (Table 2), ensuring sufficient illumination in the mixed layer. But in the autumn when the thickness of mixed layer account for about 74 % of euphotic layer, the average light intensity in the mixed layer might be influenced by the exponentially light attenuation along depth.

3.3 NCP in autumn and summer

In October 2014, NCP in the northern slope of the SCS ranged from -29.2 to 42.7 $mmol\ C\ m^{-2}\ d^{-1}$ (avg. 11.5 ± 8.7 $mmol\ C\ m^{-2}\ d^{-1}$) and most of the region was net autotrophic (Figure 4a). The estimated NCP based on the O_2/Ar values measured in this cruise is about 34 % of the net primary production rates of 34.3 $mmol\ C\ m^{-2}\ d^{-1}$ measured by ^{14}C bottle incubation (Sun X., personal communication), which was in agreement with previous research (Quay et al., 2010).

The average NCP in the study region was 11.6 ± 12.7 $mmol\ C\ m^{-2}\ d^{-1}$ with a range

of -27.6 – 61.4 $\text{mmol C m}^{-2} \text{ d}^{-1}$ in June 2015. A high NCP level was observed along Transect 3 (Figure 4b). Eddy-entrained shelf water brought a large amount of terrigenous nutrients from the shelf to the slope region along Transect 3 (He et al., 2016). The average nitrate (NO_3^-) and nitrite (NO_2^-) concentrations in the surface water of Transect 3 were 2.31 ± 0.70 $\mu\text{mol L}^{-1}$ and 0.04 ± 0.01 $\mu\text{mol L}^{-1}$ respectively (Figure S1a, S1b); both values were much higher than those found in the other three transects where NO_3^- was in a range of < 0.03 – 0.69 $\mu\text{mol L}^{-1}$ and NO_2^- was mostly below the detection limit. Li et al. (2018) reported that the entire Transect 3 and part of Transect 4 were dominated by shelf water at the surface and we estimated NCP over these regions where salinity lower than 33.0 as 23.8 ± 10.7 $\text{mmol C m}^{-2} \text{ d}^{-1}$ on average. We also observed a warm eddy (anti-cyclone) covering most stations in Transects 1 and 2 (Figure 1b, 1c) during our survey in June 2015 (Chen et al., 2016). Anti-cyclonic eddies can cause downwelling, deepening of the thermocline, and blocking of the supply of nutrients from the deeper water (Ning et al., 2008; Shi et al., 2014). Consequently, a warm eddy is expected to result in an oligotrophic condition in the surface water associated with low Chl a concentrations and low production (Ning et al., 2004). As a result, in the summer of 2015, the observed NO_2^- , NO_3^- , and PO_4^{3-} (phosphate) concentrations were almost below the detection limit in Transects 1 and 2 (Figure S1a, S1b, S1d). NCP in Transect 1 and 2 was at a very low level (avg. 2.8 ± 2.7 $\text{mmol C m}^{-2} \text{ d}^{-1}$). Because of the significant high values of NCP over the regions with shelf water intrusion, our NCP result in the summer of 2015 is averagely higher than the previous values of 4.47 $\text{mmol C m}^{-2} \text{ d}^{-1}$ and 0.17 $\text{mol C m}^{-2} \text{ month}^{-1}$ (5.67 $\text{mmol C m}^{-2} \text{ d}^{-1}$) based on DIC budget and Argo- O_2 respectively in the SCS (Chou et al., 2006; Huang et al., 2018). However, NCP estimates based on both methods mentioned above suffer from poor temporal and spatial coverage and do not allow for revealing rapid changes in shelf systems. In contrast, continuous measurements of O_2/Ar allow us to capture rapid variations in NCP along Transect 3 and resolve short-term productivity responses to environmental fluctuations.

3.4 Distribution of various parameters along representative transects

We chose Transect 5 (Figure 1a) observed in October 2014 and Transect 4 (Figure 1b) observed in June 2015 to show the distribution of various parameters.

The distribution of Chl a, $\Delta(\text{O}_2/\text{Ar})$, and NCP showed similar trend along Transect 5 in October 2014 (Figure 5). There's a trough of temperature, showing a maximum drawdown of $\sim 0.6^\circ\text{C}$ compared to the average temperature in the study region (Figure 5a). But the temperature fluctuations shown here are too small to reflect a significant upwelling that can easily cause $\sim 2^\circ\text{C}$ drawdown of temperature in the upper layer (Lin et al., 2013; Manning et al., 2017; Ning et al., 2004). A spike of Chl a occurred between 115.6°E and 115.7°E and was coincident with the peaks of $\Delta(\text{O}_2/\text{Ar})$ and NCP (Figure 5b, 5c). The highest surface concentration of ammonium (NH_4^+) of $0.35\ \mu\text{mol L}^{-1}$ was also observed between 115.6°E and 115.7°E in this transect and was predominantly higher than the concentrations ($0.07\text{--}0.17\ \mu\text{mol L}^{-1}$) in the other regions of this cruise (Figure 5c, S2b). Because no significant obduction processes (i.e., upwelling, entrainment, and diapycnal mixing) were reported in this region, the most likely source of this abundant NH_4^+ was in situ regeneration. The excretion of zooplankton and the bacterial decomposition of organic matter were considered to be the main mechanisms for the release of NH_4^+ into the surface water (La Roche, 1983; Clark et al., 2008). Ammonium is an important nitrogen source of phytoplankton growth, which can be quickly utilized by phytoplankton, and contributes to primary production (Dugdale and Goering, 1967; Tamminen, 1982). Though we only got nutrient data at two CTD stations in this transect, the result partly indicated that higher ammonium could result in higher $\Delta(\text{O}_2/\text{Ar})$ and NCP.

A similar distribution pattern of Chl a, NCP, and $\Delta(\text{O}_2/\text{Ar})$ was observed along Transect 4 in June 2015, whereas $p\text{CO}_2$ showed the opposite trend for these three parameters (Figure 6b, 6c). Low salinity (lower than 33) existed at both southern and northern end of this transect (Figure 6a). The concentration of dissolved inorganic nitrogen (DIN , $\text{NO}_3^- + \text{NO}_2^- + \text{NH}_4^+$) in the surface water was $0.81\ \mu\text{mol L}^{-1}$ and $0.27\ \mu\text{mol L}^{-1}$ at the southern and northern end respectively, which was higher than the concentrations in other stations of this transect (Figure 6c). These results indicate that shelf water is imported at the northern and southern end of this transect, along

with higher levels of Chl a and NCP (Figure 6c). A sharp drop in the temperature and an increase in salinity occurred from 19.7°N to 19.8°N and from 21°N to 20.7°N (Figure 6a), manifesting an upwelling over this area together with dramatic spikes in $p\text{CO}_2$ and associated decrease in $\Delta(\text{O}_2/\text{Ar})$ (Nemcek et al., 2008) (Figure 6b). A localized cold eddy was considered to be the cause of this upwelling (Figure 1c), and most regions of Transect 4 were dominated by upwelling and showed negative sea level height anomaly (Chen et al., 2016; He et al., 2016), resulting in a maximum temperature drawdown of $\sim 1.6^\circ\text{C}$ in the mixed layer.

Vertical mixing is considered the largest source of error in O_2/Ar -based NCP estimates because the upwelled subsurface water with different O_2/Ar signatures can produce either an overestimation or an underestimation of NCP in the mixed layer (Cassar et al., 2014; Izett et al., 2018). Former researches usually ignored the underestimated negative NCP that caused by vertical mixing (Giesbrecht et al., 2012; Reuer et al., 2007; Stanley et al., 2010). Cassar et al. (2014) presented a N_2O -based correction method of O_2/Ar and NCP for vertical mixing. Although this method has been successfully adopted by Izett et al. (2018) in the Subarctic Northeast Pacific, it is not suitable for our study region. This is because it is basically applicable in areas where the depths of euphotic zone and mixed layer are similar, and this method is not suitable for oligotrophic regions (Cassar et al., 2014). The SCS is recognized as an oligotrophic region and the depth of the euphotic zone can be 2–7 times that of the mixed layer in our study region in the summer. In addition, in the region (e.g. the SCS basin) where subsurface oxygen maximum exists, the applicability of N_2O -based correction method is limited (Izett et al., 2018). In Transect 4, the regions with negative NCP and the regions with salinity higher than 33.5 and temperature lower than 30°C are defined as influenced by upwelling. If we neglect these regions in Transect 4, the average NCP in June 2015 can slightly raise to $12.4 \pm 12.3 \text{ mmol C m}^{-2} \text{ d}^{-1}$. If we also remove the influence of shelf water intrusion by neglecting the regions with salinity lower than 33, the average NCP can sharply decrease to $5.0 \pm 6.2 \text{ mmol C m}^{-2} \text{ d}^{-1}$, which was similar to the results of $4.47 \text{ mmol C m}^{-2} \text{ d}^{-1}$ and $0.17 \text{ mol C m}^{-2} \text{ month}^{-1}$ ($5.67 \text{ mmol C m}^{-2} \text{ d}^{-1}$) reported in previous researches in the same

season (Chou et al., 2006; Huang et al., 2018). Here we regard $5.0 \pm 6.2 \text{ mmol C m}^{-2} \text{ d}^{-1}$ as the background value of NCP in the study region. Since an average NCP of $23.8 \pm 10.7 \text{ mmol C m}^{-2} \text{ d}^{-1}$ was observed over the regions with salinity lower than 33, we can conclude that the summer shelf water intrusion significantly promoted NCP by about 376 % in June 2015.

3.5 Factors influencing NCP in the SCS

The SCS is an oligotrophic region with low biomass and primary production (Lee Chen, 2005; Ning et al., 2004). Previous research has shown that the nutrient, especially nitrogen and phosphorus, is the most important factor controlling and limiting the phytoplankton biomass and primary production in the SCS (Ning et al., 2004; Lee Chen, 2005; Lee Chen and Chen, 2006; Han et al., 2013). After neglecting the two CTD stations (J-14, J-15) with negative NCP influenced by upwelling in June 2015, we performed a principal component analysis (PCA) to determine the dominant factors influencing NCP in both cruises. In October 2014, DIN (0.741), $\Delta(\text{O}_2/\text{Ar})$ (0.858), and NCP (0.979) were significantly loaded on Factor 1, indicating a potential relationship among these three variables (Figure 7a, Table S1b). The correlation coefficient between DIN and NCP was 0.706 ($p < 0.01$, Table S1a), which was significantly higher than the coefficient between NCP and the other variables, except for $\Delta(\text{O}_2/\text{Ar})$ and temperature; this indicated that DIN was an important factor influencing NCP in this cruise. Another two nutrients – dissolved silicate (DSi, SiO_3^{2-}) and dissolved inorganic phosphorus (DIP, PO_4^{3-}) – had no correlations ($p > 0.05$) with NCP (Table S1a). In June 2015, Factor 1 showed a strong loading by DIN (0.876), Chl a (0.950), DO (0.927), $\Delta(\text{O}_2/\text{Ar})$ (0.902), and NCP (0.909), whereas salinity (−0.936) and $p\text{CO}_2$ (−0.908) were negatively loaded on Factor 1 (Figure 7b, Table S2b). The injection of low salinity shelf water appeared to have a strong effect on the study region because significant negative correlations were observed between salinity and DIN, Chl a, $\Delta(\text{O}_2/\text{Ar})$, and NCP (Table S2a). DIN had strong correlations with NCP, $\Delta(\text{O}_2/\text{Ar})$, and Chl a, with the correlation coefficients of 0.747, 0.910, and 0.754, respectively (Table S2a), indicating that DIN was the dominant factor controlling the

growth of phytoplankton and primary production in this cruise. DSi (0.582) and DIP (−0.601) were both moderately loaded on Factor 2 (Figure 7b, Table S2b) and had no correlations with NCP ($p > 0.05$, Table S2a). These results suggested the key role of nitrogen in regulating $\Delta(\text{O}_2/\text{Ar})$, NCP, and phytoplankton biomass in the SCS. The supply of nitrogen may stimulate the growth of phytoplankton in the SCS and nitrogen is an important participant in photosynthesis and a basic element that contributes to the increase in primary production (Dugdale and Goering, 1967; Lee Chen, 2005; Lee Chen and Chen, 2006; Han et al., 2013).

Coupled with biochemical variations, physical processes also play important roles in the slope region of the SCS by transporting abundant nutrient-rich shelf water into the SCS and bringing deep water to the surface by enhancing water mixing (Chen and Tang, 2012; Ning et al., 2004; Pan et al., 2012). The surface waters in the slope region of the northern SCS are primarily composed of waters originating from SCS water, Kuroshio water, and shelf water (Li et al., 2018). In the summer, the shelf water exists where the potential density anomaly is lower than 20.5 kg m^{-3} (Li et al., 2018). In the autumn, there is a weak offshore transport of the shelf water in the SCS and the salinity of the water mixed with the shelf water is usually lower than 33 (Fan et al., 1988; Uu and Brankart, 1997; Su and Yuan, 2005). In October 2014, the observed surface salinity was in a range of 33.28 to 34.11; thus the surface waters were mainly derived from mixing of the Kuroshio water and the SCS water. In the summer of 2015, a cyclonic-anticyclonic eddy pair was observed in the study region (Figure 1c). Low-salinity shelf water mixed with the intruding plume water from the Pearl River in the upper 50 m and was transported to the slope and basin along the intersection of the two eddies (Chen et al., 2016; He et al., 2016; Li et al., 2018). In both seasons, the surface waters in the study region were generally found to be nitrogen deficient, with NO_2^- at $< 0.01\text{--}0.04 \text{ } \mu\text{mol L}^{-1}$ (Figure S2a, S1b), NO_3^- at $< 0.03\text{--}2.82 \text{ } \mu\text{mol L}^{-1}$ (Figure S1a), and NH_4^+ at $0.04\text{--}0.35 \text{ } \mu\text{mol L}^{-1}$ (Figure S2b, S1c). The concentrations of NO_2^- and NO_3^- were below the detection limit at almost 80% of the sampling stations during both cruises. Due to the injection of shelf water with low salinity and abundant terrestrial nutrients, significant high concentrations of NO_3^- and NO_2^- were

observed along Transect 3 in June 2015 (Figure S1a, S1b) where the shelf water was intruded by eddies (Chen et al., 2016; He et al., 2016). Such transport processes from the inner shelf to the slope region have a profound influence on nutrient dynamics and biological productions (He et al., 2016). The water that was influenced by shelf water with a potential density anomaly lower than 20.25 kg m^{-3} and salinity lower than 33.0 had high concentrations of DIN (Figure 8a). At the 6 stations (in the red circle of Figure 8a) that were intruded by shelf water and characterized with surface salinity lower than 33.0, we obtained an average surface DIN concentration of 1.82 ± 1.16 ($0.27\text{--}3.01$) $\mu\text{mol L}^{-1}$, which was significantly higher than the mean of 0.10 ± 0.03 ($0.04\text{--}0.16$) $\mu\text{mol L}^{-1}$ at other stations (independent samples t-test, $p < 0.01$). After neglecting the two stations (J-14, J-15) influenced by upwelling, a strong correlation between NCP and DIN was observed during the cruise of June 2015 ($r = 0.747$, $p < 0.01$), with higher NCP (avg. $15.4 \pm 4.5 \text{ mmol C m}^{-2} \text{ d}^{-1}$) occurred at the stations where shelf water intruded, consistent with the DIN concentration higher than $0.27 \mu\text{mol L}^{-1}$ (Figure 8b). At other stations without the influence of shelf water, the average NCP was just $2.3 \pm 1.7 \text{ mmol C m}^{-2} \text{ d}^{-1}$. These results furtherly suggest that the supply of DIN from shelf water can greatly stimulate the primary production at these stations, resulting in the NCP increase of nearly 7 times compared to other stations.

The correlations between NCP and sea surface temperature and salinity also support the influence of physical forcing on NCP. In June 2015, we obtained strong negative correlations between NCP and salinity (Figure 9d). NCP significantly increased in the water with salinity lower than 33 (Figure 9d). Temperature had weak correlations with NCP (Figure 9c), and the negative NCP values were concentrated in the water with temperatures below 30.5°C and salinity values over 33.5 (Figure 9c, 9d). This surface water was mostly observed along Transect 4 where vertical mixing caused by a cold eddy brought deep water to the surface. The undersaturated $\Delta(\text{O}_2/\text{Ar})$ entrained by deep water caused the negative NCP estimates at the surface, resulting in a considerable underestimation of NCP. Unlike in June 2015, all the correlations were very weak between NCP and temperature, salinity in October 2014 (Figure 9a, 9b).

The Kuroshio water and the SCS water had similar hydrological characteristics and their mixing in October 2014 may not have resulted in significant changes in the hydrological characteristics of the surface water.

The nutrient concentrations and hydrographic characteristics we observed just reflect the marine environment at the moment of sampling, partly contradicting our estimates that quantified NCP over a period prior to the observation. Especially for the regions with significant influence of shelf water in June 2015, tracking the history of shelf water intrusion is important. We used daily satellite Chl *a* to monitor the movement of shelf water and roughly set $\text{Chl } a \geq \sim 0.2 \mu\text{g L}^{-1}$ as the criterion of shelf water (Figure S3). On 10 June 2015, the shelf water began to influence the northern end (J-9) of Transect 3 and most part of Transect 4, then it extended to the southern end of Transect 3 and Transect 4 where J-12 and J-13 located on 13 June (Figure 1b, S3). Till 25 June when we finished the observation of Transect 4, the entire Transect 3 (J-9 to 12) as well as J-13 and J-16 had kept been dominated by shelf water for more than 10 days (Figure 1b, S3). We concluded these findings in Table 3, along with the mixed layer O_2 residence time (τ) and the difference (Δday) between the date of observation and the start date of shelf water intrusion at stations with surface salinity lower than 33. Δday can represent the duration of the shelf water intrusion at each station before our observation. The mixed layer O_2 residence time at most stations listed in Table 3 is shorter than or equivalent to Δday . This result suggests that our estimate has appropriately integrated the NCP during the period of shelf water intrusion, which can effectively reflect the influence of shelf water on productive state on the northern slope of SCS in the summer.

Light may also play a role in the primary production. The MLD is considered a driver of light availability in the mixed layer (Cassar et al., 2011; Hahm et al., 2014). The euphotic layer was averagely 40 m thicker than the mixed layer in the study region during the summer cruise, thus it's not very significant to discuss the light limitation in June 2015. We conducted an analysis of light availability based on daily satellite-PAR data and NCP in October 2014. To minimize the influence of DIN concentrations, we selected 9 stations where surface DIN concentration in the range

of 0.10–0.17 $\mu\text{mol L}^{-1}$. The average surface PAR ($\text{mol m}^{-2} \text{d}^{-1}$) at each station was integrated over the residence time of O_2 before our observation. Then an average PAR in the mixed layer was calculated based on K_d . At the selected stations, the surface PAR varies over a range of 38.6–42.2 $\text{mol m}^{-2} \text{d}^{-1}$, while the average PAR in the mixed layer (ML PAR) ranged from 8.7 to 13.3 $\text{mol m}^{-2} \text{d}^{-1}$ (Table 4). There's no significant correlation between the average PAR and NCP in the mixed layer (Table 4), partly suggesting that light intensity may not be a factor on NCP in the autumn. Light availability in the northern slope region of SCS is enough to support the primary production of phytoplankton.

4 Conclusion

The distribution of $\Delta(\text{O}_2/\text{Ar})$ and NCP on the northern slope of the SCS was strongly affected by nutrient availability, especially nitrogen. The nitrogen limitation on NCP was found both in the autumn and summer. In June 2015, we observed strong biological responses to the supply of nitrogen induced by eddy-entrained shelf water intrusion. NCP in the region with the influence of shelf water was $23.8 \pm 10.7 \text{ mmol C m}^{-2} \text{d}^{-1}$ on average, with a maximum of 61.4 $\text{mmol C m}^{-2} \text{d}^{-1}$. In addition, dynamic processes such as vertical mixing caused the errors of NCP estimates. Removing the regions with the influence of shelf water intrusion and vertical mixing, the average NCP in other regions was $5.0 \pm 6.2 \text{ mmol C m}^{-2} \text{d}^{-1}$. This value agrees well with previously published NCP estimates for the study area. Our results also reveal the rapid response of ecosystem to physical processes. The summer shelf water intrusion may significantly promote NCP by 376 % in the study region. This is the first report that quantifies the contribution of shelf water intrusion to NCP on the northern slope of the SCS in the summer. Because of the sufficient illumination in the tropical SCS, light availability may not be a significant limitation on NCP in both seasons. The high-resolution NCP estimates derived from continuous measurements of O_2/Ar presented in this paper are of significance for understanding the carbon cycling in the highly dynamic system of the SCS.

566

567 **Data Availability**

568 All data presented in this manuscript are available on Weiyun.com (link:
569 <https://share.weiyun.com/ZtbQMNGI>, password: p7rj36)

570 **Author contribution**

571 Guiling Zhang and Yu Han designed and set up the underway measurement system.
572 Wenjing Zheng attended both cruises (in June 2015 and October 2014) in the South
573 China Sea, and was mainly responsible for operating the underway measurement
574 system during the cruises. Sumei Liu provided the nutrients data of both cruises.
575 Chuan Qin attended the cruise in June 2015 and prepared the manuscript with
576 contributions from all co-authors.

577 **Acknowledgments**

578 The authors wish to thank the crew of the *R/V “Nanfeng”* for the assistance with the
579 collection of field samples and Professor Xiaoxia Sun for providing the ^{14}C -PP data.
580 Professor Michael Bender and Bror Jonsson are acknowledged for constructive
581 suggestions on the continuous O_2/Ar measurement system and the calculation of
582 O_2/Ar -based NCP. This study was funded by the National Science Foundation of
583 China through Grant Nos. 41776122, by the Ministry of Science and Technology of
584 China through Grant Nos. 2014CB441502, by the Fundamental Research Funds for
585 the Central Universities (No. 201562010), and by the Taishan Scholars Programme of
586 Shandong Province (No. 201511014) and the Aoshan Talents Programme of the
587 Qingdao National Laboratory for Marine Science and Technology (No.
588 2015ASTP-OS08).

589 **Competing interests**

590 The authors declare that they have no conflict of interest.

591

References:

- Bi, Q., Du, J., Wu, Y., Zhou, J. and Zhang, J.: Particulate organic carbon export flux by $^{234}\text{Th}/^{238}\text{U}$ disequilibrium in the continental slope of the East China Sea, *Acta Oceanol. Sin.*, 32(10), 67–73, doi:10.1007/s13131-013-0303-7, 2013.
- Cai, P., Zhao, D., Wang, L., Huang, B. and Dai, M.: Role of particle stock and phytoplankton community structure in regulating particulate organic carbon export in a large marginal sea, *J. Geophys. Res. Oceans*, 120(3), 2063–2095, doi:10.1002/2014JC010432, 2015.
- Cai, W.: Estuarine and Coastal Ocean Carbon Paradox: CO_2 Sinks or Sites of Terrestrial Carbon Incineration?, *Ann. Rev. Mar. Sci.*, 3(1), 123–145, doi:10.1146/annurev-marine-120709-142723, 2011.
- Cassar, N., Difiore, P. J., Barnett, B. A., Bender, M. L., Bowie, A. R., Tilbrook, B., Petrou, K., Westwood, K. J., Wright, S. W. and Lefevre, D.: The influence of iron and light on net community production in the Subantarctic and Polar Frontal Zones, *Biogeosciences*, 8(2), 227–237, doi:10.5194/bg-8-227-2011, 2011.
- Cassar, N., Nevison, C. D. and Manizza, M.: Correcting oceanic O_2/Ar -net community production estimates for vertical mixing using N_2O observations, *Geophys. Res. Lett.*, 41(24), 8961–8970, doi:10.1002/2014GL062040, 2014.
- Chen, J., Zheng, L., Wiesner, M. G., Chen, R., Zheng, Y. and Wong, H.: Estimations of primary production and export production in the South China Sea based on sediment trap experiments, *Chinese Sci. Bull.*, 43(7), 583–586, doi:10.1007/BF02883645, 1998.
- Chen, W., Cai, P., Dai, M. and Wei, J.: $^{234}\text{Th}/^{238}\text{U}$ disequilibrium and particulate organic carbon export in the northern South China Sea, *J. Oceanogr.*, 64(3), 417–428, doi:10.1007/s10872-008-0035-z, 2008.
- Chen, Y. and Tang, D.: Eddy-feature phytoplankton bloom induced by a tropical cyclone in the South China Sea, *Int. J. Remote Sens.*, 33(23), 7444–7457, doi:10.1080/01431161.2012.685976, 2012.
- Chen, Z., Yang, C., Xu, D. and Xu, M.: Observed hydrographical features and circulation with influences of cyclonic-anticyclonic eddy-pair in the northern slope of the South China Sea during June 2015 (in Chinese), *J. Mar. Sci.*, 34(4), 10–19, doi:10.3969/j.issn.1001-909X.2016.04.002,

2016.

Cheng, G., Sun, J., Zu, T., Chen, J. and Wang, D.: Analysis of water masses in the northern South China Sea in summer 2011 (in Chinese), *J. Trop. Oceanogr.*, 33(3), 10–16, doi:10.3969/j.issn.1009-5470.2014.03.002, 2014.

Chou, W., Lee Chen, Y., Sheu, D., Shih, Y., Han, C., Cho, C., Tseng, C. and Yang, Y.: Estimated net community production during the summertime at the SEATS time-series study site, northern South China Sea: Implications for nitrogen fixation, *Geophys. Res. Lett.*, 33(22), doi:10.1029/2005GL025365, 2006.

Clark, D. R., Rees, A. P. and Joint, I.: Ammonium regeneration and nitrification rates in the oligotrophic Atlantic Ocean: Implications for new production estimates, *Limnol. Oceanogr.*, 53(1), 52–62, doi:10.4319/lo.2008.53.1.0052, 2008.

Craig, H. and Hayward, T.: Oxygen Supersaturation in the Ocean: Biological Versus Physical Contributions, *Science*, 235(4785), 199–202, doi:10.1126/science.235.4785.199, 1987.

Dugdale, R. C. and Goering, J. J.: Uptake of New and Regenerated Forms of Nitrogen in Primary Productivity, *Limnol. Oceanogr.*, 12(2), 196–206, doi:10.4319/lo.1967.12.2.0196, 1967.

Eveleth, R., Cassar, N., Sherrell, R. M., Ducklow, H., Meredith, M. P., Venables, H. J., Lin, Y. and Li, Z.: Ice melt influence on summertime net community production along the Western Antarctic Peninsula, *Deep Sea Res. Part II Top. Stud. Oceanogr.*, 139, 89–102, doi:10.1016/j.dsr2.2016.07.016, 2017.

Fan, L., Su, Y. and Li, F.: Analysis on water masses in the Northern South China Sea (in Chinese), *Acta Oceanol. Sin.*, 10(2), 136–145, 1988.

Feng, S., Li, F. and Li, S.: An introduction to marine science (in Chinese), Higher Education Press, Beijing, China., 1999.

Giesbrecht, K. E., Hamme, R. C. and Emerson, S. R.: Biological productivity along Line P in the subarctic northeast Pacific: In situ versus incubation-based methods, *Global Biogeochem. Cycles*, 26(3), doi:10.1029/2012GB004349, 2012.

Grande, K. D., Williams, P. J. L. B., Marra, J., Purdie, D. A., Heinemann, K., Eppley, R. W. and Bender, M. L.: Primary production in the North Pacific gyre: a comparison of rates determined by the ^{14}C , O_2 concentration and ^{18}O methods, *Deep Sea Res. Part A, Oceanogr. Res. Pap.*, 36(11), 1621–1634, doi:10.1016/0198-0149(89)90063-0, 1989.

651 Guéguen, C. and Tortell, P. D.: High-resolution measurement of Southern Ocean CO₂ and O₂/Ar
 652 by membrane inlet mass spectrometry, *Mar. Chem.*, 108(3–4), 184–194,
 653 doi:10.1016/j.marchem.2007.11.007, 2008.

654 Hahm, D., Rhee, T. S., Kim, H. C., Park, J., Kim, Y. N., Shin, H. C. and Lee, S.: Spatial and
 655 temporal variation of net community production and its regulating factors in the Amundsen Sea,
 656 Antarctica, *J. Geophys. Res. Oceans*, 119(5), 2815–2826, doi:10.1002/2013JC009762, 2014.

657 Hamme, R. C., Cassar, N., Lance, V. P., Vaillancourt, R. D., Bender, M. L., Strutton, P. G., Moore,
 658 T. S., DeGrandpre, M. D., Sabine, C. L., Ho, D. T. and Hargreaves, B. R.: Dissolved O₂/Ar and
 659 other methods reveal rapid changes in productivity during a Lagrangian experiment in the
 660 Southern Ocean, *J. Geophys. Res. Oceans*, 117(C4), 92–99, doi:10.1029/2011JC007046, 2012.

661 Han, A., Dai, M., Gan, J., Kao, S., Zhao, X., Jan, S., Li, Q., Lin, H., Chen, C., Wang, L., Hu, J.,
 662 Wang, L. and Gong, F.: Inter-shelf nutrient transport from the East China Sea as a major nutrient
 663 source supporting winter primary production on the northeast South China Sea shelf,
 664 *Biogeosciences*, 10(12), 8159–8170, doi:10.5194/bg-10-8159-2013, 2013.

665 Hanson, C. E., Pesant, S., Waite, A. M. and Pattiaratchi, C. B.: Assessing the magnitude and
 666 significance of deep chlorophyll maxima of the coastal eastern Indian Ocean, *Deep. Res. Part II*
 667 *Top. Stud. Oceanogr.*, 54(8–10), 884–901, doi:10.1016/j.dsr2.2006.08.021, 2007.

668 He, X., Xu, D., Bai, Y., Pan, D., Chen, C. A., Chen, X. and Gong, F.: Eddy-entrained Pearl River
 669 plume into the oligotrophic basin of the South China Sea, *Cont. Shelf Res.*, 124, 117–124,
 670 doi:10.1016/j.csr.2016.06.003, 2016.

671 Hu, J., Kawamura, H., Hong, H. and Qi, Y.: A Review on the currents in the South China Sea:
 672 Seasonal circulation, South China Sea warm current and Kuroshio intrusion, *J. Oceanogr.*, 56(6),
 673 607–624, doi:10.1023/A:1011117531252, 2000.

674 Huang, Y., Yang, B., Chen, B., Qiu, G., Wang, H. and Huang, B.: Net community production in
 675 the South China Sea Basin estimated from in situ O₂ measurements on an Argo profiling float,
 676 *Deep Sea Res. Part I Oceanogr. Res. Pap.*, 131, 54–61, doi:10.1016/j.dsr.2017.11.002, 2018.

677 Izett, R. W., Manning, C. C., Hamme, R. C. and Tortell, P. D.: Refined Estimates of Net
 678 Community Production in the Subarctic Northeast Pacific Derived From ΔO₂/Ar Measurements
 679 With N₂O-Based Corrections for Vertical Mixing, *Global Biogeochem. Cycles*, 32(3), 326–350,
 680 doi:10.1002/2017GB005792, 2018.

681 Jiang, Z., Huang, C., Dai, M., Kao, S., Hydes, D. J., Chou, W. and Janf, S.: Short-term dynamics
 682 of oxygen and carbon in productive nearshore shallow seawater systems off Taiwan: Observations
 683 and modeling, *Limnol. Oceanogr.*, 56(5), 1832–1849, doi:10.4319/lo.2011.56.5.1832, 2011.
 684 Jonsson, B. F., Doney, S. C., Dunne, J. and Bender, M.: Evaluation of the Southern Ocean
 685 O₂/Ar-based NCP estimates in a model framework, *J. Geophys. Res. Biogeosciences*, 118(2),
 686 385–399, doi:10.1002/jgrg.20032, 2013.
 687 Jerlov, N. G.: *Marine optics*, Elsevier, Netherlands, 1976.
 688 Kaiser, J., Reuer, M. K., Barnett, B. and Bender, M. L.: Marine productivity estimates from
 689 continuous O₂/Ar ratio measurements by membrane inlet mass spectrometry, *Geophys. Res. Lett.*,
 690 32(19), 1–5, doi:10.1029/2005GL023459, 2005.
 691 Kirk, J. T.: *Light and photosynthesis in aquatic ecosystems*, Cambridge university press, UK,
 692 1994.
 693 La Roche, J.: Ammonium regeneration: its contribution to phytoplankton nitrogen requirements in
 694 a eutrophic environment, *Mar. Biol.*, 75(2–3), 231–240, doi:10.1007/BF00406007, 1983.
 695 Lee Chen, Y.: Spatial and seasonal variations of nitrate-based new production and primary
 696 production in the South China Sea, *Deep Sea Res. Part I Oceanogr. Res. Pap.*, 52(2), 319–340,
 697 doi:10.1016/j.dsr.2004.11.001, 2005.
 698 Lee Chen, Y. and Chen, H.: Seasonal dynamics of primary and new production in the northern
 699 South China Sea: The significance of river discharge and nutrient advection, *Deep Sea Res. Part I*
 700 *Oceanogr. Res. Pap.*, 53(6), 971–986, doi:10.1016/j.dsr.2006.02.005, 2006.
 701 Li, D., Zhou, M., Zhang, Z., Zhong, Y., Zhu, Y., Yang, C., Xu, M., Xu, D. and Hu, Z.: Intrusions
 702 of Kuroshio and Shelf Waters on Northern Slope of South China Sea in Summer 2015, *J. Ocean*
 703 *Univ. China*, 17(3), 477–486, doi:10.1007/s11802-018-3384-2, 2018.
 704 Li, Q., Guo, X., Zhai, W., Xu, Y. and Dai, M.: Partial pressure of CO₂ and air-sea CO₂ fluxes in
 705 the South China Sea: Synthesis of an 18-year dataset, *Prog. Oceanogr.*, 182,
 706 doi:10.1016/j.pocean.2020.102272, 2020.
 707 Liao, X., Dai, M., Gong, X., Liu, X. and Huang, H.: Subsurface chlorophyll a maximum and its
 708 possible causes in the southern South China Sea, *J. Trop. Oceanogr.*, 37(1), 45–56,
 709 doi:10.11978/2017020, 2018.
 710 Lin, X., Guan, Y. and Liu, Y.: Three-dimensional structure and evolution process of Dongsha Cold

711 Eddy during autumn 2000 (in Chinese), *J. Trop. Oceanogr.*, 32(2), 55–65,
 712 doi:10.3969/j.issn.1009-5470.2013.02.006, 2013.

713 Liu, M., Liu, X., Ma, A., Li, T. and Du, Z.: Spatio-temporal stability and abnormality of
 714 chlorophyll-a in the northern south china sea during 2002-2012 from MODIS images using
 715 wavelet analysis, *Cont. Shelf Res.*, 75, 15–27, doi:10.1016/j.csr.2013.12.010, 2014.

716 Lockwood, D., Quay, P. D., Kavanaugh, M. T., Juranek, L. W. and Feely, R. A.: High-resolution
 717 estimates of net community production and air-sea CO₂ flux in the northeast Pacific, *Global*
 718 *Biogeochem. Cycles*, 26(4), doi:10.1029/2012GB004380, 2012.

719 Ma, H., Zeng, Z., He, J., Chen, L., Yin, M., Zeng, S. and Zeng, W.: Vertical flux of particulate
 720 organic carbon in the central South China Sea estimated from ²³⁴Th-²³⁸U disequilibria, *Chinese J.*
 721 *Oceanol. Limnol.*, 26(4), 480–485, doi:10.1007/s00343-008-0480-y, 2008.

722 Ma, H., Zeng, Z., Yu, W., He, J., Chen, L., Cheng, J., Yin, M. and Zeng, S.: ²³⁴Th/ ²³⁸U
 723 disequilibrium and particulate organic carbon export in the northwestern South China Sea, *Acta*
 724 *Oceanol. Sin.*, 30(3), 55–62, doi:10.1007/s13131-011-0119-2, 2011.

725 Manning, C. C., Stanley, R. H. R., Nicholson, D. P., Smith, J. M., Timothy Pennington, J.,
 726 Fewings, M. R., Squibb, M. E. and Chavez, F. P.: Impact of recently upwelled water on
 727 productivity investigated using in situ and incubation-based methods in Monterey Bay, *J. Geophys.*
 728 *Res. Oceans*, 122(3), 1901–1926, doi:10.1002/2016JC012306, 2017.

729 Mathis, J. T., Cross, J. N. and Bates, N. R.: Coupling primary production and terrestrial runoff to
 730 ocean acidification and carbonate mineral suppression in the eastern Bering Sea, *J. Geophys. Res.*
 731 *Ocean.*, 116(2), doi:10.1029/2010JC006453, 2011.

732 Millero, F. J. and Poisson, A.: International one-atmosphere equation of state of seawater, *Deep*
 733 *Sea Res. Part A, Oceanogr. Res. Pap.*, 28(6), 625–629, doi:10.1016/0198-0149(81)90122-9, 1981.

734 Monterey, G. and Levitus, S.: Seasonal Variability of Mixed Layer Depth, NOAA Atlas NEDIS
 735 14, U.S. Gov. Printng Off. D.C. [online] Available from: <http://www.nodc.noaa.gov>, 1997.

736 Nemcek, N., Ianson, D. and Tortell, P. D.: A high-resolution survey of DMS, CO₂, and O₂/Ar
 737 distributions in productive coastal waters, *Global Biogeochem. Cycles*, 22(2),
 738 doi:10.1029/2006GB002879, 2008.

739 Ning, X., Chai, F., Xue, H., Cai, Y., Liu, C. and Shi, J.: Physical-biological oceanographic
 740 coupling influencing phytoplankton and primary production in the South China Sea, *J. Geophys.*

741 Res. Oceans, 109(10), doi:10.1029/2004JC002365, 2004.
 742 Ning, X., Peng, X., Le, F., Hao, Q., Sun, J., Liu, C. and Cai, Y.: Nutrient limitation of
 743 phytoplankton in anticyclonic eddies of the northern South China Sea, Biogeosciences Discuss.,
 744 5(6), 4591–4619, doi:10.5194/bgd-5-4591-2008, 2008.
 745 Pan, X., Wong, G. T. F., Shiah, F. K. and Ho, T. Y.: Enhancement of biological productivity by
 746 internal waves: Observations in the summertime in the northern South China Sea, J. Oceanogr.,
 747 68(3), 427–437, doi:10.1007/s10872-012-0107-y, 2012.
 748 Parsons, T. R., Maita, Y. and Lalli, C. M.: A Manual of Chemical & Biological Methods for
 749 Seawater Analysis, Pergamon Press, Oxford, UK., 1984.
 750 Quay, P. D., Peacock, C., Bjrkman, K. and Karl, D. M.: Measuring primary production rates in the
 751 ocean: Enigmatic results between incubation and non-incubation methods at Station ALOHA,
 752 Global Biogeochem. Cycles, 24(3), doi:10.1029/2009GB003665, 2010.
 753 Rehder, G. and Suess, E.: Methane and $p\text{CO}_2$ in the Kuroshio and the South China Sea during
 754 maximum summer surface temperatures, Mar. Chem., 75(1–2), 89–108,
 755 doi:10.1016/S0304-4203(01)00026-3, 2001.
 756 Reuer, M. K., Barnett, B. A., Bender, M. L., Falkowski, P. G. and Hendricks, M. B.: New
 757 estimates of Southern Ocean biological production rates from O_2/Ar ratios and the triple isotope
 758 composition of O_2 , Deep Sea Res. Part I Oceanogr. Res. Pap., 54(6), 951–974,
 759 doi:10.1016/j.dsr.2007.02.007, 2007.
 760 Shadwick, E. H., Tilbrook, B., Cassar, N., Trull, T. W. and Rintoul, S. R.: Summertime physical
 761 and biological controls on O_2 and CO_2 in the Australian Sector of the Southern Ocean, J. Mar.
 762 Syst., 147, 21–28, doi:10.1016/j.jmarsys.2013.12.008, 2015.
 763 Shi, X., Li, H., Han, X., Wang, L. and Zhu, C.: Influence of typical mesoscale oceanographical
 764 process on the distribution of nutrients and dissolved oxygen in the Northern part of South China
 765 Sea in summer (in Chinese), Acta Sci. Circumstantiae, 34(3), 695–703,
 766 doi:10.13671/j.hjkxxb.2014.0121, 2014.
 767 Stanley, R. H. R., Kirkpatrick, J. B., Cassar, N., Barnett, B. A. and Bender, M. L.: Net community
 768 production and gross primary production rates in the western equatorial Pacific, Global
 769 Biogeochem. Cycles, 24(4), doi:10.1029/2009GB003651, 2010.
 770 Su, J. and Yuan, Y.: Coastal hydrology of China (in Chinese), China Ocean Press, Beijing, China.,

2005.

Takahashi, T., Sutherland, S. C., Wanninkhof, R., Sweeney, C., Feely, R. A., Chipman, D. W., Hales, B., Friederich, G., Chavez, F., Sabine, C., Watson, A., Bakker, D. C. E., Schuster, U., Metzl, N., Yoshikawa-Inoue, H., Ishii, M., Midorikawa, T., Nojiri, Y., Körtzinger, A., Steinhoff, T., Hoppema, M., Olafsson, J., Arnarson, T. S., Tilbrook, B., Johannessen, T., Olsen, A., Bellerby, R., Wong, C. S., Delille, B., Bates, N. R. and de Baar, H. J. W.: Climatological mean and decadal change in surface ocean $p\text{CO}_2$, and net sea–air CO_2 flux over the global oceans, Deep Sea Res. Part II Top. Stud. Oceanogr., 56(8–10), 554–577, doi:10.1016/j.dsr2.2008.12.009, 2009.

Tamminen, T.: Effects of ammonium effluents on planktonic primary production and decomposition in a coastal brackish water environment I. Nutrient balance of the water body and effluent tests, Netherlands J. Sea Res., 16(C), 455–464, doi:10.1016/0077-7579(82)90050-3, 1982.

Teeter, L., Hamme, R. C., Ianson, D. and Bianucci, L.: Accurate Estimation of Net Community Production From O_2/Ar Measurements, Global Biogeochem. Cycles, 32(8), 1163–1181, doi:10.1029/2017GB005874, 2018.

Teira, E., Mouriño, B., Maraño, E., Pérez, V., Pazó, M. J., Serret, P., De Armas, D., Escánez, J., Woodward, E. M. S. and Fernández, E.: Variability of chlorophyll and primary production in the Eastern North Atlantic Subtropical Gyre: Potential factors affecting phytoplankton activity, Deep. Res. Part I Oceanogr. Res. Pap., 52(4), 569–588, doi:10.1016/j.dsr.2004.11.007, 2005.

Tortell, P. D.: Dissolved gas measurements in oceanic waters made by membrane inlet mass spectrometry, Limnol. Oceanogr. Methods, 3(1), 24–37, doi:10.4319/lom.2005.3.24, 2005.

Tortell, P. D., Asher, E. C., Ducklow, H. W., Goldman, J. A. L., Dacey, J. W. H., Grzyski, J. J., Young, J. N., Kranz, S. A., Bernard, K. S. and Morel, F. M. M.: Metabolic balance of coastal Antarctic waters revealed by autonomous $p\text{CO}_2$ and $\Delta\text{O}_2/\text{Ar}$ measurements, Geophys. Res. Lett., 41(19), 6803–6810, doi:10.1002/2014GL061266, 2014.

Tortell, P. D., Merzouk, A., Ianson, D., Pawlowicz, R. and Yelland, D. R.: Influence of regional climate forcing on surface water $p\text{CO}_2$, $\Delta\text{O}_2/\text{Ar}$ and dimethylsulfide (DMS) along the southern British Columbia coast, Cont. Shelf Res., 47, 119–132, doi:10.1016/j.csr.2012.07.007, 2012.

Ulfso, A., Cassar, N., Korhonen, M., Van Heuven, S., Hoppema, M., Kattner, G. and Anderson, L. G.: Late summer net community production in the central Arctic Ocean using multiple approaches, Global Biogeochem. Cycles, 28(10), 1129–1148, doi:10.1002/2014GB004833, 2014.

801 Uu, D. V. and Brankart, J. M.: Seasonal variation of temperature and salinity fields and water
 802 masses in the Bien Dong (South China) Sea, *Math. Comput. Model.*, 26(12), 97–113,
 803 doi:10.1016/S0895-7177(97)00243-4, 1997.
 804 Wang, N., Lin, W., Cheng, B. and Huang, B.: Metabolic states of the Taiwan Strait and the
 805 northern South China Sea in summer 2012 (in Chinese), *J. Trop. Oceanogr.*, 33(4), 61–68,
 806 doi:10.3969/j.issn.1009-5470.2014.04.008, 2014.
 807 Wanninkhof, R.: Relationship between wind speed and gas exchange over the ocean, *J. Geophys.*
 808 *Res. Oceans*, 97(C5), 7373–7382, doi:10.1029/92JC00188, 1992.
 809 Weiss, R. F.: The solubility of nitrogen, oxygen and argon in water and seawater, *Deep Sea Res.*
 810 *Oceanogr. Abstr.*, 17(4), 721–735, doi:10.1016/0011-7471(70)90037-9, 1970.
 811 Zhai, W., Dai, M. and Cai, W.: Coupling of surface $p\text{CO}_2$ and dissolved oxygen in the northern
 812 South China Sea: Impacts of contrasting coastal processes, *Biogeosciences*, 6(11), 2589–2598,
 813 doi:10.5194/bg-6-2589-2009, 2009.
 814 Zhang, R., Zhu, X., Yang, C., Ye, L., Zhang, G., Ren, J., Wu, Y., Liu, S., Zhang, J. and Zhou, M.:
 815 Distribution of dissolved iron in the Pearl River (Zhujiang) Estuary and the northern continental
 816 slope of the South China Sea, *Deep. Res. Part II Top. Stud. Oceanogr.*, 167, 14–24,
 817 doi:10.1016/j.dsr2.2018.12.006, 2019.
 818
 819

820 **Table Captions:**

821 **Table 1.** Basic information at all CTD stations in October 2014

822 **Table 2.** Basic information at all CTD stations in June 2015

823 **Table 3.** The start date and duration (Δ day) of shelf water intrusion at stations with surface salinity
824 lower than 33 in June 2015

825 **Table4.** Satellite-PAR data and NCP at selected stations in October 2014

826

Figure Captions:

Figure 1. Cruise tracks of two cruises in the slope region of the Northern South China Sea in (a) October 2014, (b) June 2015. The sea level height anomaly (SLA) and geostrophic current during observations in June 2015 (Chen et al., 2016) are shown in (c). The black dots/stars represent the locations of the CTD casts. Red numbers indicate transects, while black numbers indicate the serial number of CTD stations based on the cruise plan. The color scale in (a) and (b) represents bathymetry.

Figure 2. Surface distributions of (a) temperature, (b) salinity, (c) chlorophyll-a (Chl a), and (d) $\Delta(\text{O}_2/\text{Ar})$ in October 2014

Figure 3. Surface distributions of (a) temperature, (b) salinity, (c) chlorophyll-a (Chl a), (d) dissolved oxygen (DO), (e) $p\text{CO}_2$, and (f) $\Delta(\text{O}_2/\text{Ar})$ in June 2015

Figure 4. Surface distribution of NCP among the northern slope of SCS during the cruise in (a) October 2014 and (b) June 2015.

Figure 5. Zonal variations in (a) temperature, salinity, (b) $\Delta(\text{O}_2/\text{Ar})$, (c) Chl a, NCP and surface concentration of ammonia (NH_4^+) along Transect 5 in October 2014. The plots of $\Delta(\text{O}_2/\text{Ar})$ and NCP are 10-point Savitzky-Golay smoothed to give a better view of their distribution.

Figure 6. Meridional variations in (a) temperature, salinity, (b) $\Delta(\text{O}_2/\text{Ar})$, $p\text{CO}_2$, (c) Chl a, NCP and surface concentration of DIN along Transect 4 in June 2015. The plots of $\Delta(\text{O}_2/\text{Ar})$, $p\text{CO}_2$ and NCP are 10-point Savitzky-Golay smoothed.

Figure 7. Principal Component Analysis (PCA) among variables for (a) October 2014 and (b) June 2015 (Bartlett's test of sphericity: $p < 0.01$)

Figure 8. (a) T-S diagram of surface DIN concentration in June 2015. The stations influenced by shelf water were in the red circle. (b) Correlation analysis between surface DIN concentration and NCP at sampling stations. The stations (characterized with $S < 33$) influenced by shelf water presented surface DIN concentration $\geq 0.27 \mu\text{mol L}^{-1}$.

Figure 9. Correlation analysis between underway NCP and physical parameters (temperature and salinity) in October 2014 (a, b) and June 2015 (c, d).

Table 1. Basic information at all CTD stations in October 2014

Station	Date of observation ^a	MLD (m)	Z _{eu} ^b (m)	k ^c (m d ⁻¹)	τ^d (d)
O-01	2014/10/13	58	82	4.7	12
O-02	2014/10/13	64	74	5.2	12
O-03	2014/10/14	56	84	6.2	9
O-04	2014/10/14	54	76	6.3	9
O-05	2014/10/20	27	70	7.9	3
O-06	2014/10/19	55	62	8.4	7
O-07	2014/10/21	40	60	7.3	5
O-08	2014/10/21	49	72	7.4	7
O-09	2014/10/15	79	96	6.2	13
O-10	2014/10/15	68	81	6.1	11
O-11	2014/10/15	64	81	5.4	12
O-12	2014/10/16	66	74	5.2	13
O-13	2014/10/16	48	52	6.3	8
O-14	2014/10/17	54	62	6.9	8
O-15	2014/10/22	49	68	7.0	7
O-16	2014/10/22	50	73	7.3	7
O-17	2014/10/23	52	75	7.9	7
O-19	2014/10/18	31	64	9.4	3
O-20	2014/10/18	35	61	8.7	4
O-21	2014/10/18	81	86	6.9	12
O-22	2014/10/17	76	102	6.0	13

^a All dates are in the format of year/month/day. ^b Euphotic depth, defined based on subsurface chlorophyll maximum layer. ^c Gas transfer velocity of O₂. ^d Residence time of O₂ in the mixed layer, estimated as per MLD/k.

854

Table 2. Basic information at all CTD stations in June 2015

Station	Date of observation	MLD (m)	Z_{eu} (m)	k (m d⁻¹)	τ (d)
J-01	2015/6/18	26	63	2.2	12
J-02	2015/6/17	19	80	1.9	10
J-03	2015/6/16	20	74	1.9	11
J-04	2015/6/15	22	74	1.9	11
J-05	2015/6/15	11	78	1.2	9
J-06	2015/6/14	24	76	2.1	11
J-07	2015/6/13	21	81	2.3	9
J-08	2015/6/18	14	56	1.7	8
J-09	2015/6/19	17	59	1.6	10
J-10	2015/6/19	8	46	1.4	6
J-11	2015/6/20	8	40	2.8	3
J-12	2015/6/21	16	45	3.0	5
J-13	2015/6/21	19	45	2.3	8
J-14	2015/6/24	28	55	4.0	7
J-15	2015/6/24	17	42	5.3	3
J-16	2015/6/25	10	19	5.7	2

855

856

857
858
859

Table 3. The start date and duration (Δ day) of shelf water intrusion at stations with surface salinity lower than 33 in June 2015

Station	Date of observation	Start date of shelf water intrusion	Δ day ^a	τ (d)
J-09	2015/6/19	2015/6/10	9	10
J-10	2015/6/19	2015/6/13	6	6
J-11	2015/6/20	2015/6/13	7	3
J-12	2015/6/21	2015/6/13	8	5
J-13	2015/6/21	2015/6/13	8	8
J-16	2015/6/25	before 2015/6/10	> 15	2

^a The difference between the date of observation and the start date of shelf water intrusion at listed stations.

Table 4. Satellite-PAR data and NCP at selected stations in October 2014

Station	Date of observation	MLD (m)	Z _{eu} (m)	Surface PAR ^a (mol m ⁻² d ⁻¹)	K _d (m ⁻¹)	ML PAR ^b (mol m ⁻² d ⁻¹)	NCP (mmol C m ⁻² d ⁻¹)
O-01	2014/10/13	58	82	42.0	5.6 * 10 ⁻²	12.0	3.0
O-02	2014/10/13	64	74	42.0	6.2 * 10 ⁻²	10.0	15.1
O-03	2014/10/14	56	84	41.1	5.5 * 10 ⁻²	12.4	10.1
O-08	2014/10/21	49	72	38.7	6.4 * 10 ⁻²	11.4	15.7
O-10	2014/10/15	68	81	40.0	5.7 * 10 ⁻²	9.8	4.4
O-13	2014/10/16	48	52	39.2	8.9 * 10 ⁻²	8.7	15.3
O-15	2014/10/22	49	68	38.6	6.8 * 10 ⁻²	10.8	16.3
O-20	2014/10/18	35	61	39.2	7.5 * 10 ⁻²	13.3	16.4
O-22	2014/10/17	76	102	42.2	4.5 * 10 ⁻²	11.6	15.7

^a Average surface PAR over the residence time of O₂ in the mixed layer. ^b Average PAR in the mixed layer.

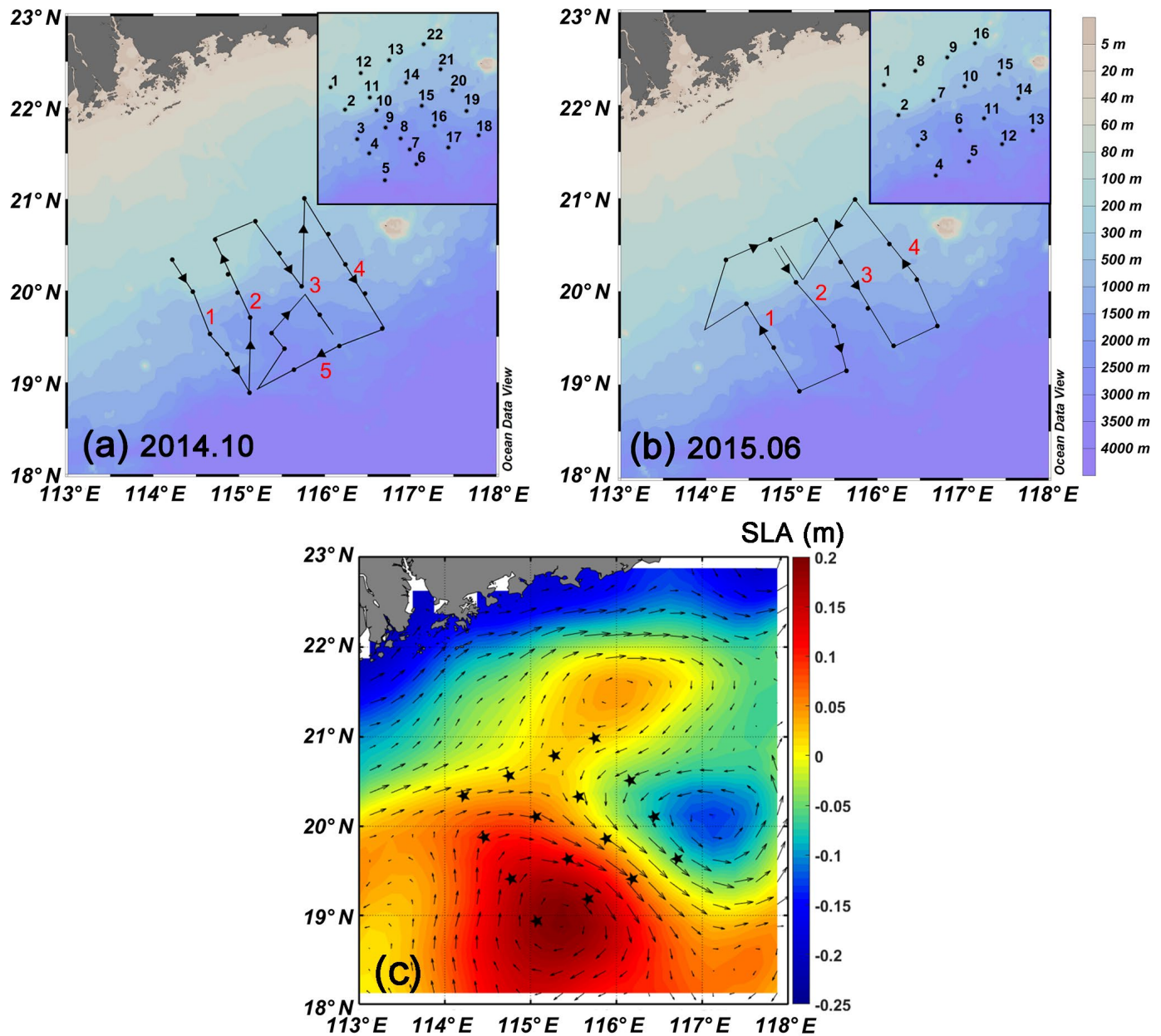


Figure 1. Cruise tracks of two cruises in the slope region of the Northern South China Sea in (a) October 2014, (b) June 2015. The sea level height anomaly (SLA) and geostrophic current during observations in June 2015 (Chen et al., 2016) are shown in (c). The black dots/stars represent the locations of the CTD casts. Red numbers indicate transects, while black numbers indicate the serial number of CTD stations based on the cruise plan. The color scale in (a) and (b) represents bathymetry.

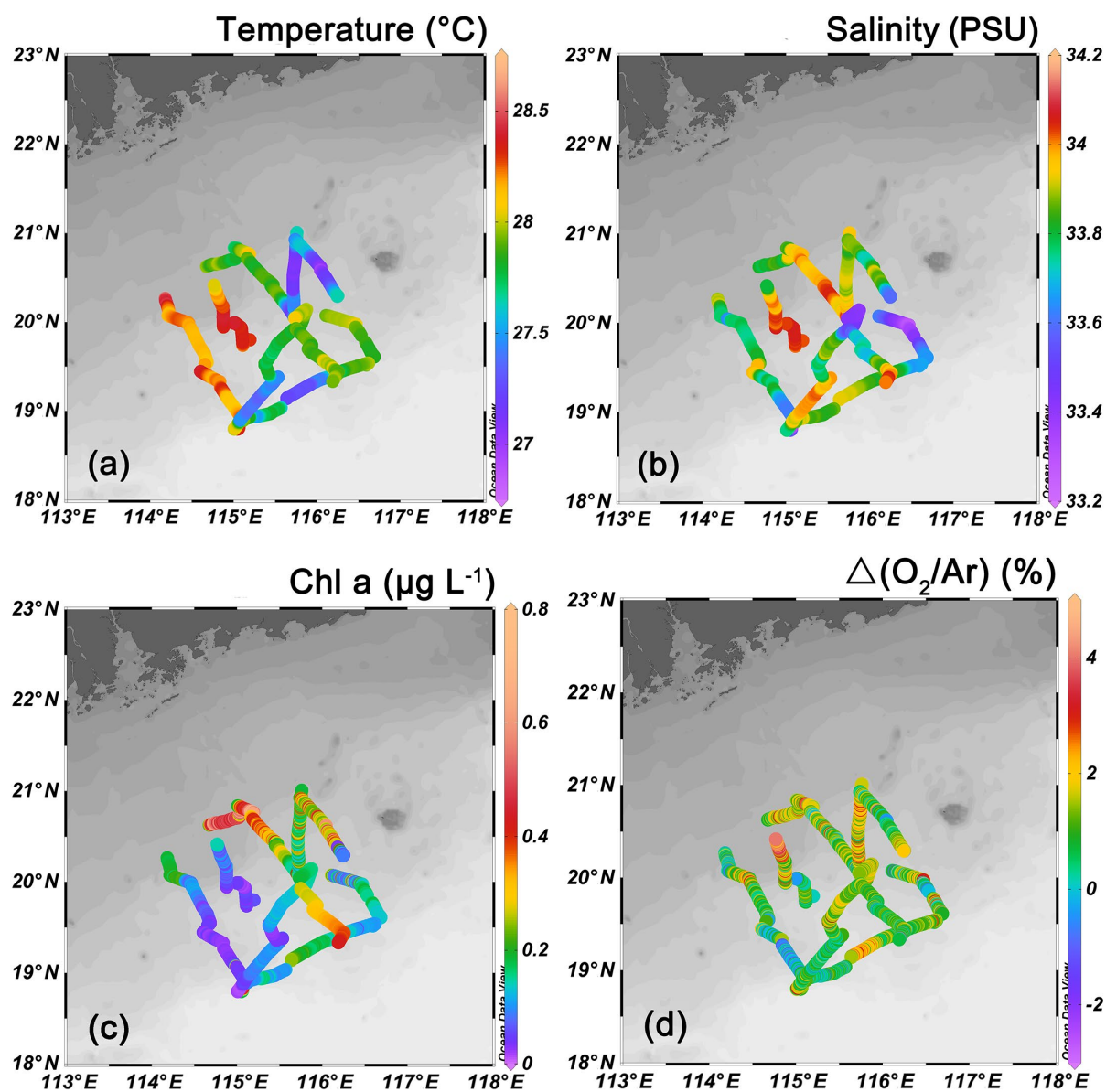


Figure 2. Surface distributions of (a) temperature, (b) salinity, (c) chlorophyll-a (Chl a), and (d) $\Delta(\text{O}_2/\text{Ar})$ in October 2014

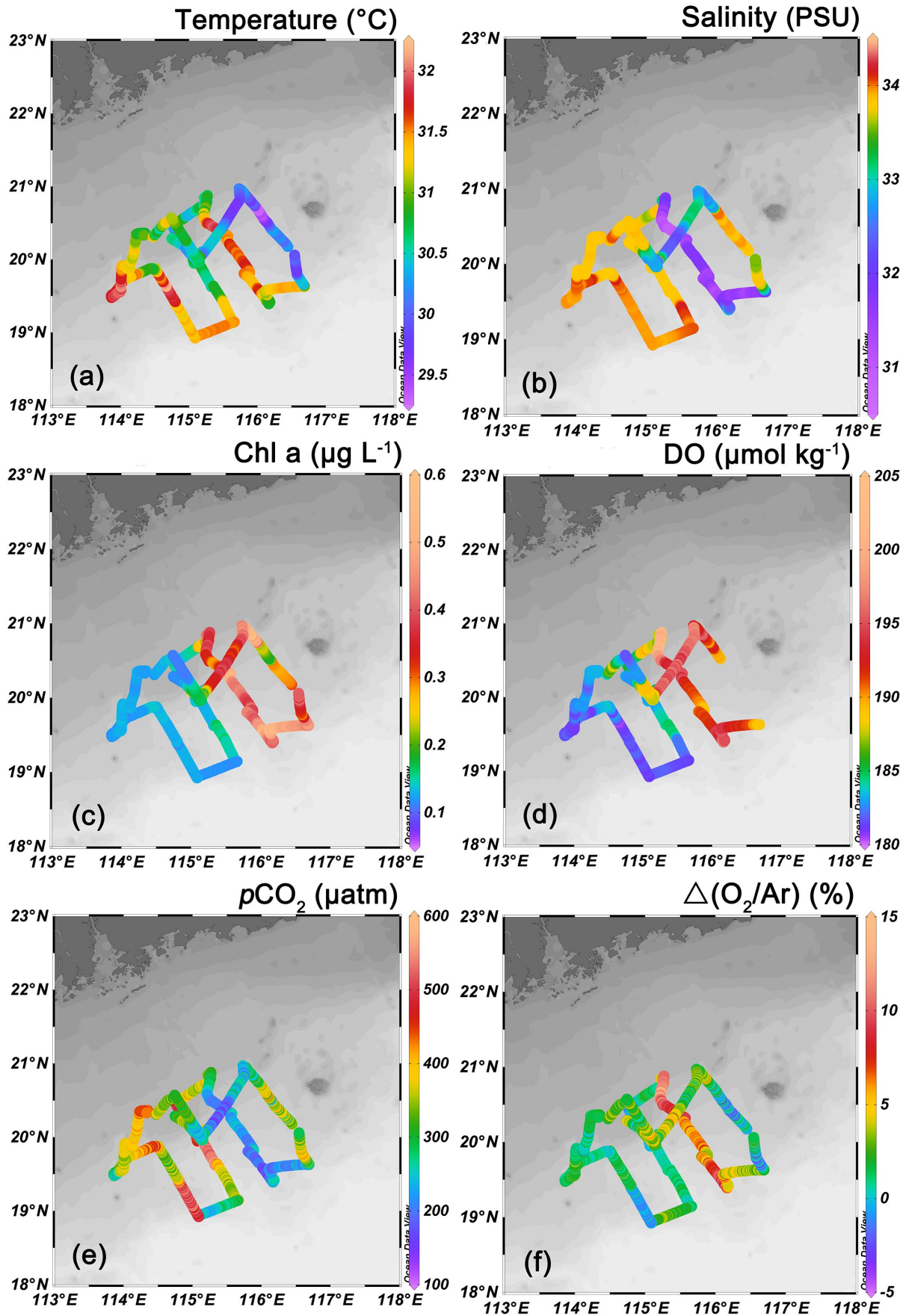


Figure 3. Surface distributions of (a) temperature, (b) salinity, (c) chlorophyll-a (Chl a), (d) dissolved oxygen (DO), (e) $p\text{CO}_2$, and (f) $\Delta(\text{O}_2/\text{Ar})$ in June 2015

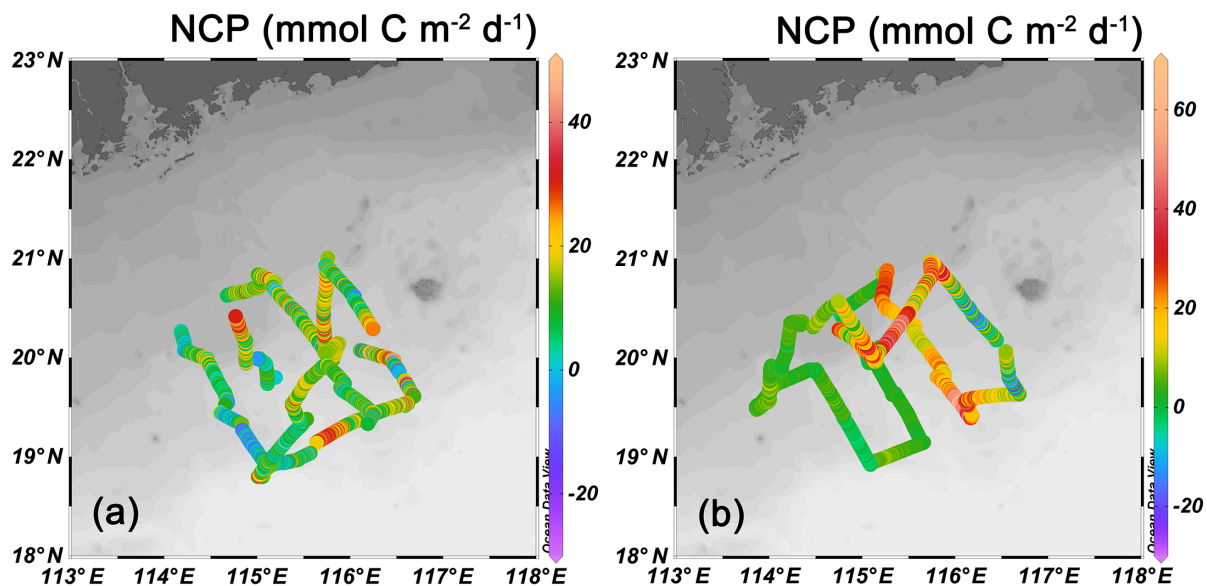


Figure 4. Surface distribution of NCP among the northern slope of SCS during the cruise in **(a)** October 2014 and **(b)** June 2015.

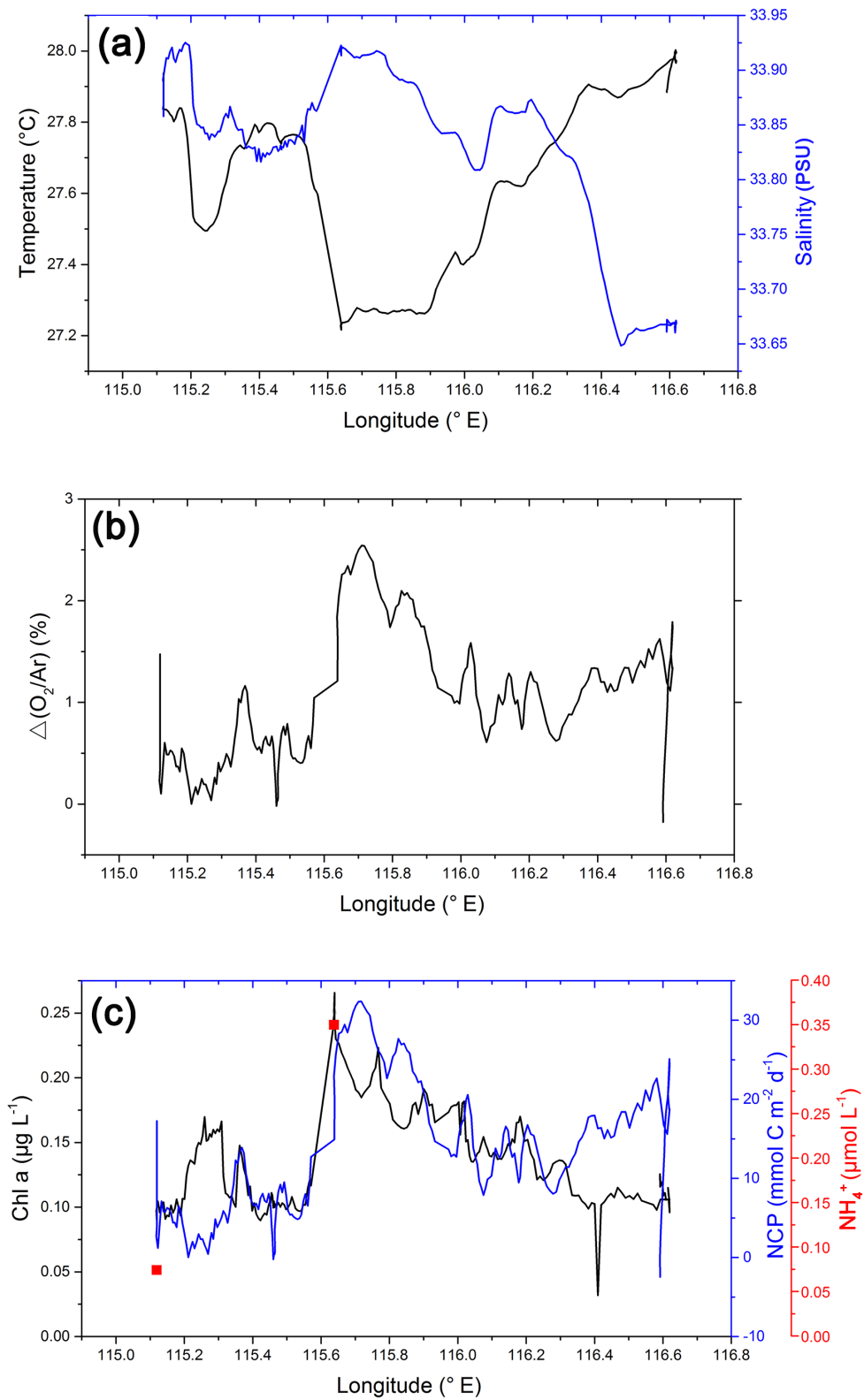


Figure 5. Zonal variations in (a) temperature, salinity, (b) $\Delta(O_2/Ar)$, (c) Chl a, NCP and surface concentration of ammonia (NH_4^+) along Transect 5 in October 2014. The plots of $\Delta(O_2/Ar)$ and NCP are 10-point Savitzky-Golay smoothed to give a better view of their distribution.

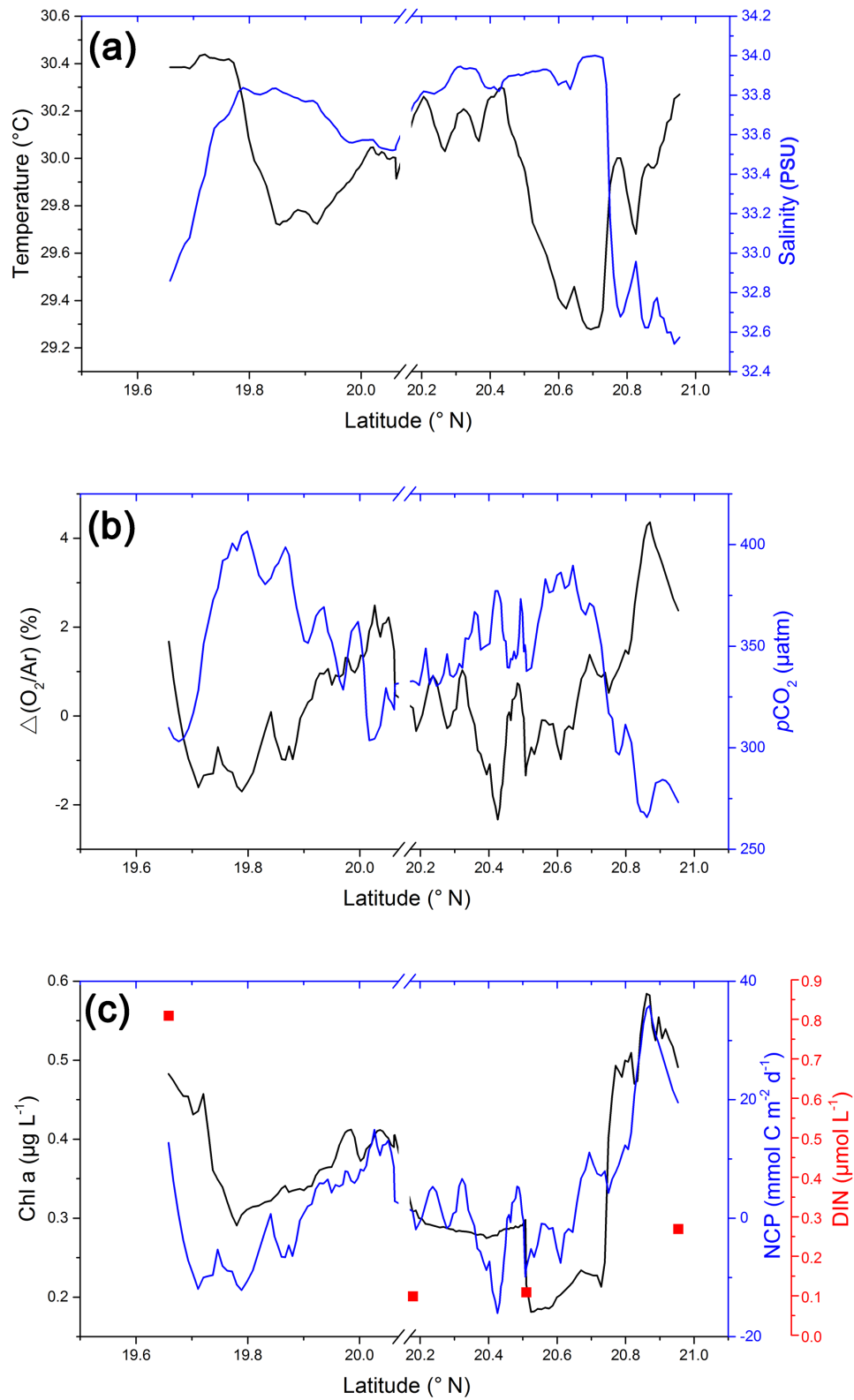


Figure 6. Meridional variations in **(a)** temperature, salinity, **(b)** $\Delta(\text{O}_2/\text{Ar})$, $p\text{CO}_2$, **(c)** Chl a, NCP and surface concentration of DIN along Transect 4 in June 2015. The plots of $\Delta(\text{O}_2/\text{Ar})$, $p\text{CO}_2$ and NCP are 10-point Savitzky-Golay smoothed.

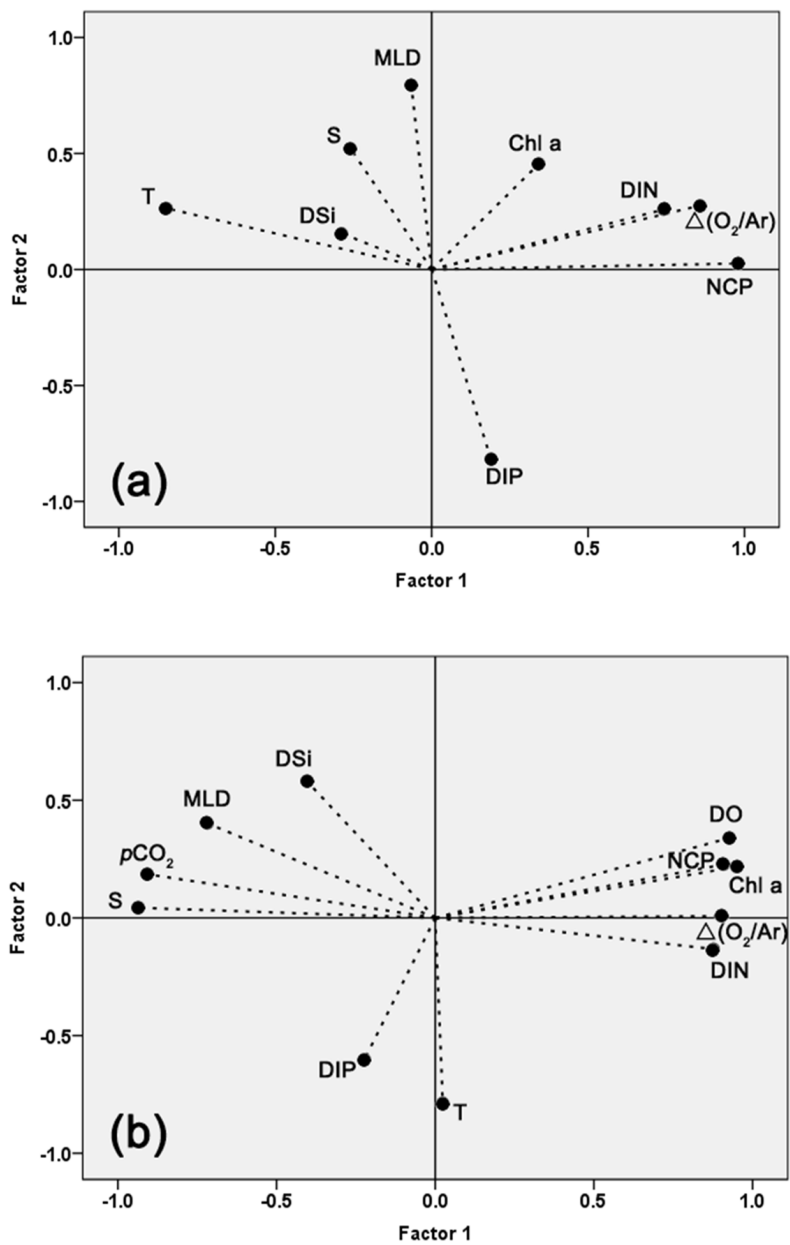


Figure 7. Principal Component Analysis (PCA) among variables for **(a)** October 2014 and **(b)** June 2015 (Bartlett's test of sphericity: $p < 0.01$)

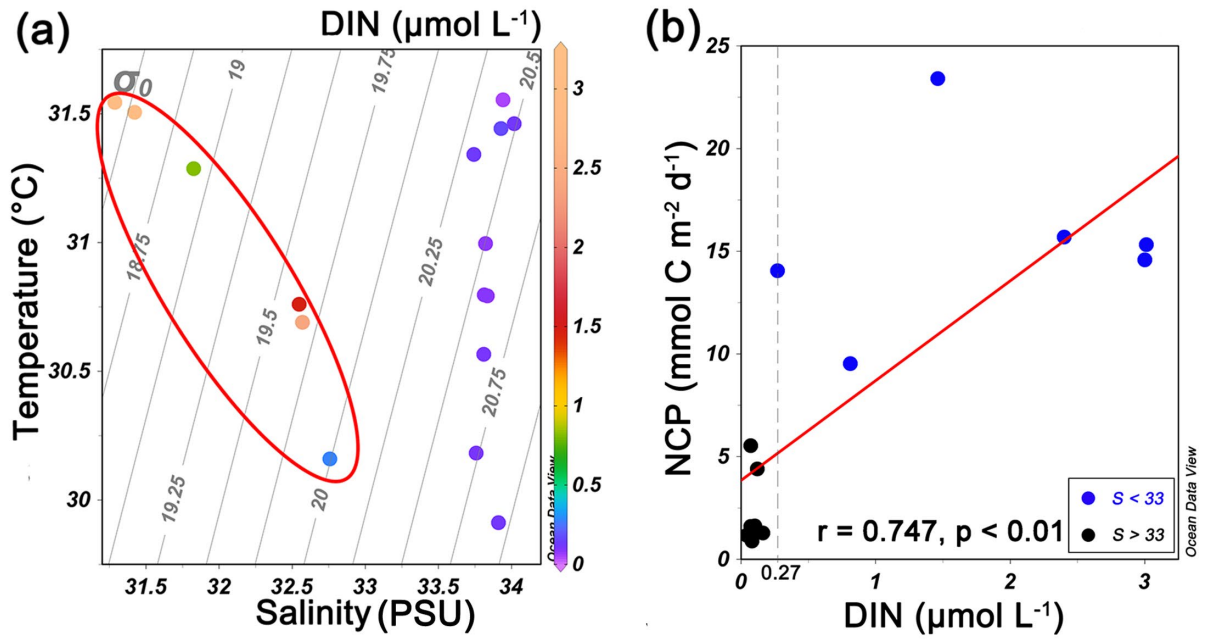


Figure 8. (a) T-S diagram of surface DIN concentration in June 2015. The stations influenced by shelf water were in the red circle. (b) Correlation analysis between surface DIN concentration and NCP at sampling stations. The stations (characterized with $S < 33$) influenced by shelf water presented surface DIN concentration $\geq 0.27 \mu\text{mol L}^{-1}$.

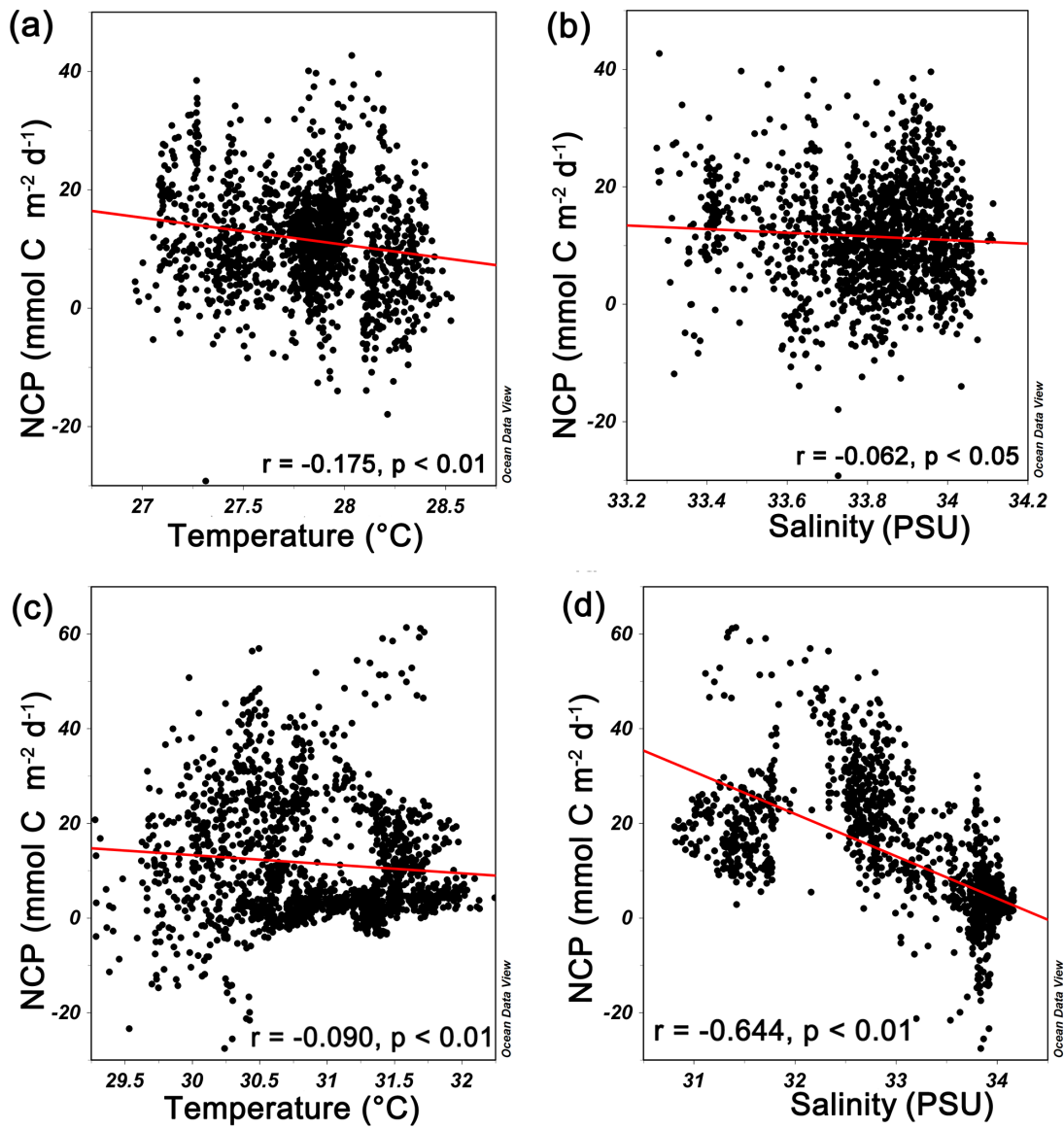


Figure 9. Correlation analysis between underway NCP and physical parameters (temperature and salinity) in October 2014 (a, b) and June 2015 (c, d).